Jetted AGN (radio loud AGN)

Partly following RL AGN lesson by P. Grandi for the Astrophysics Laboratory course

AGN classification: jetted vs. not-jetted AGN

RQ: radio quiet - RL: radio loud

$$R_L = \frac{F(5GHz)}{F(4400\mathring{A})} > 10$$

Radio over optical emission

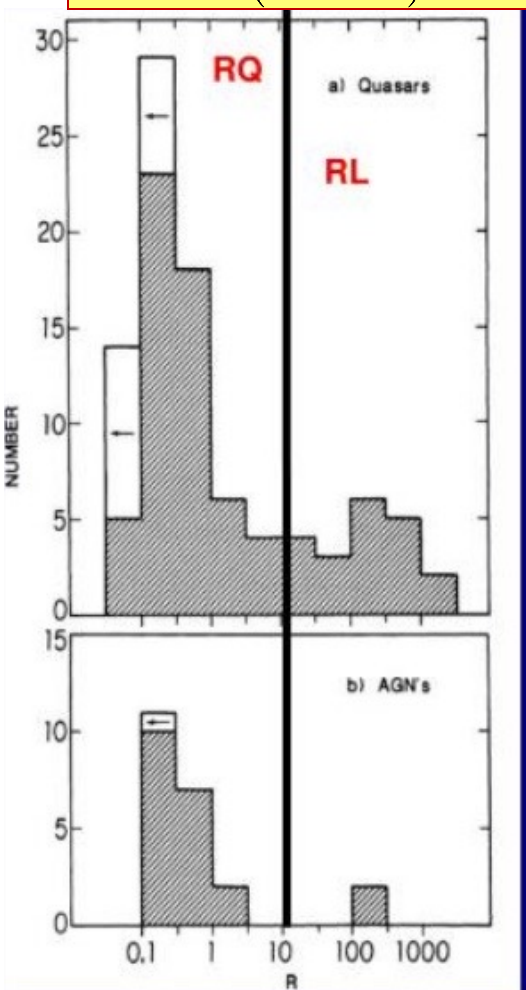

Kellerman et al. (1989)

$$logR_X = \frac{\nu \ L_\nu(5GHz)}{L_X} > -4.5$$

Radio over X-ray emission

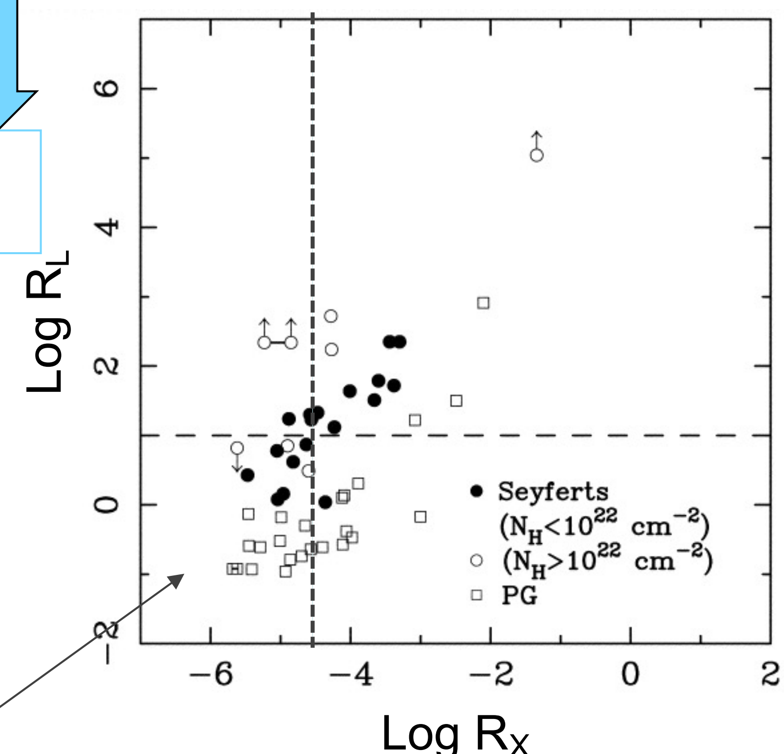

Not perfect agreements
Limitations in both definitions

Terashima & Wilson (2003)

Jetted AGN. I

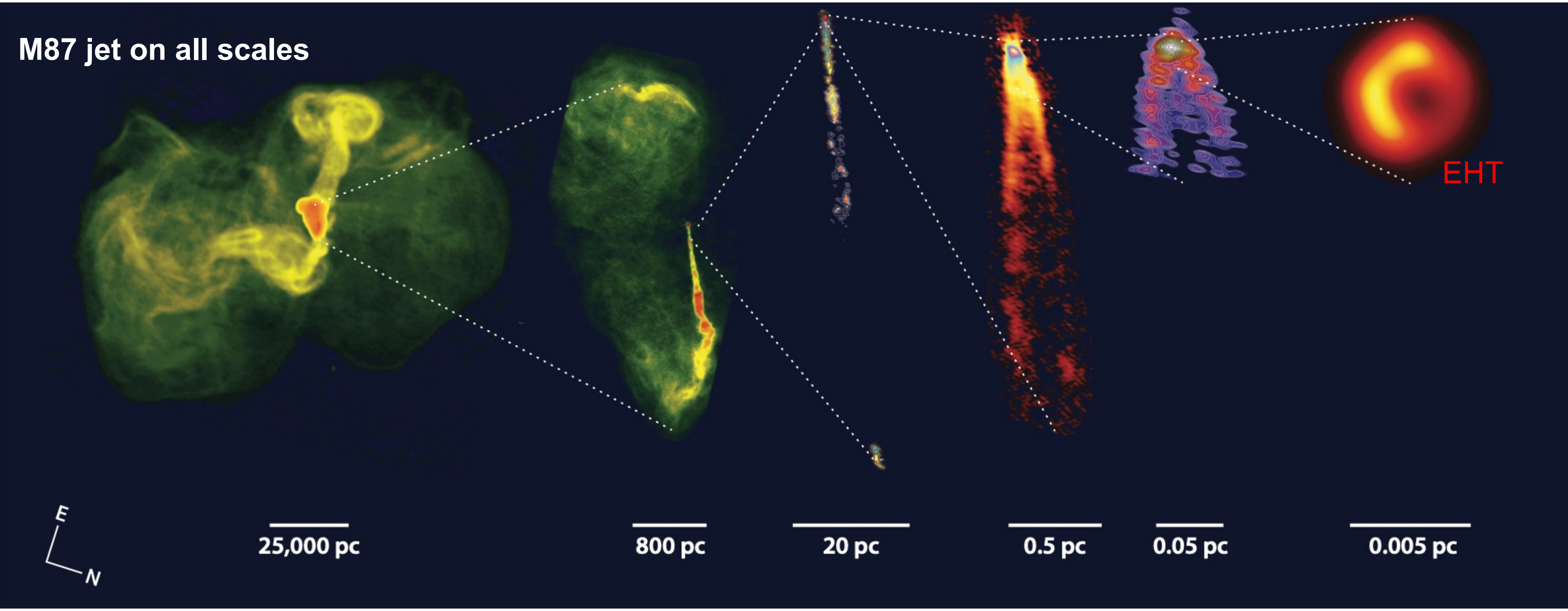

Blandford et al. (2019, ARA&A)

RL (jetted) AGN mostly in elliptical and RQ-AGN mostly in spirals

Jetted AGN. II

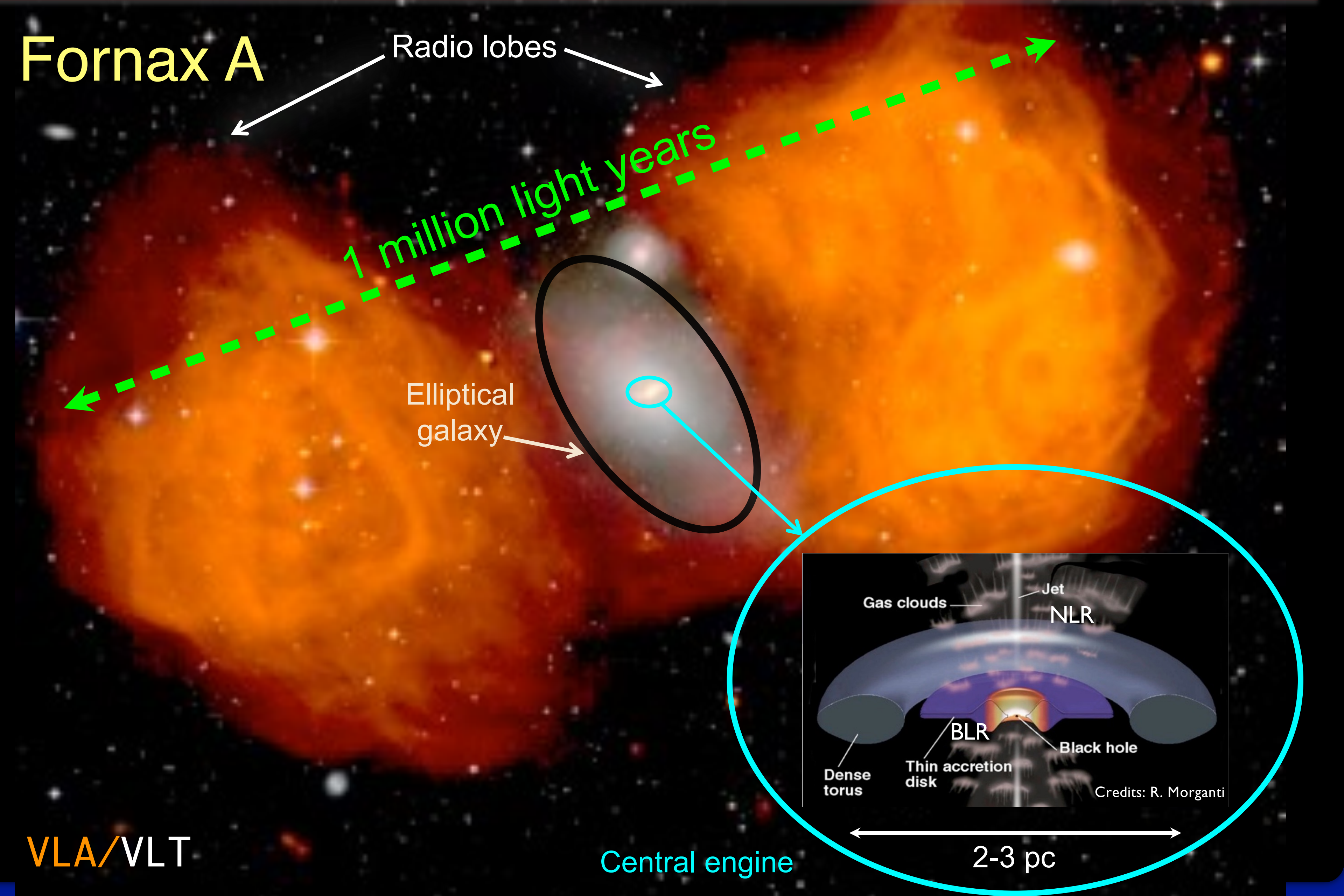

Jetted AGN. III

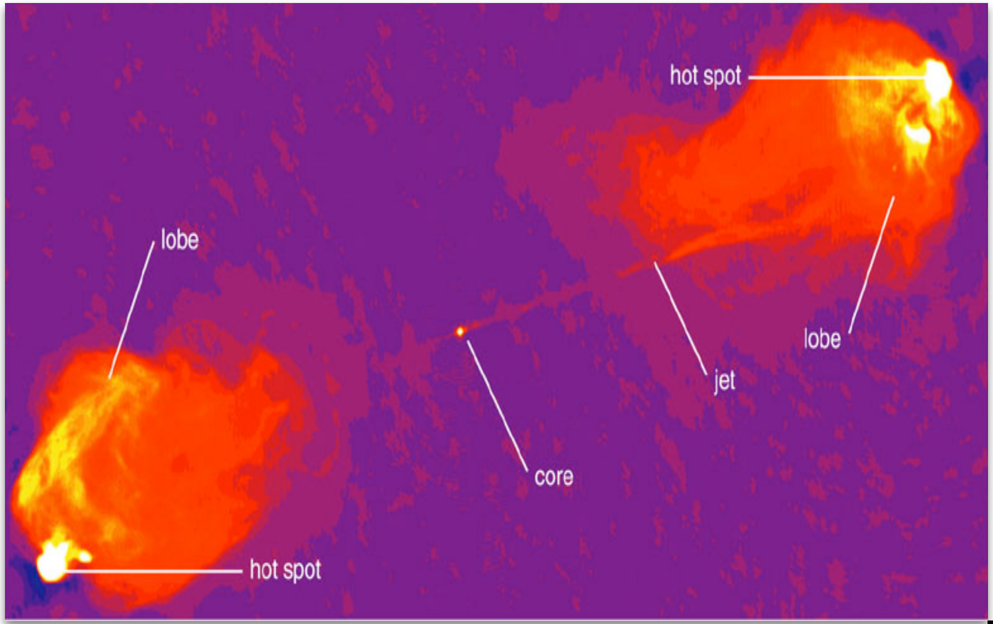

Extended emission, a lot of spatial components and spectral complexities

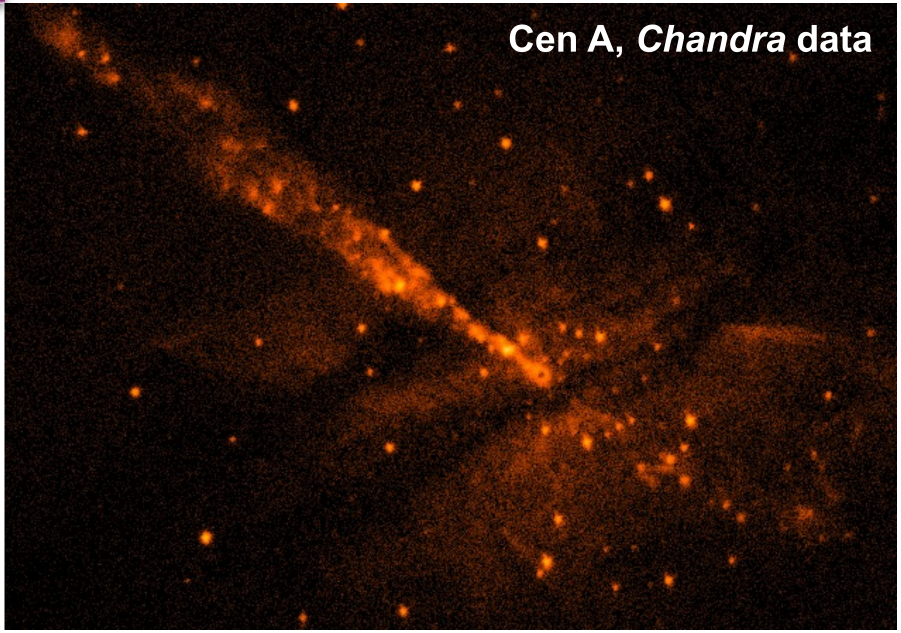

AGN optical classification. I

Already discussed in the AGN classification lesson

Broad-line (Type 1) AGN

Typically, blue optical continuum (big blue bump, emission from the accretion disc) and broad permitted emission lines (several thousand km/s)

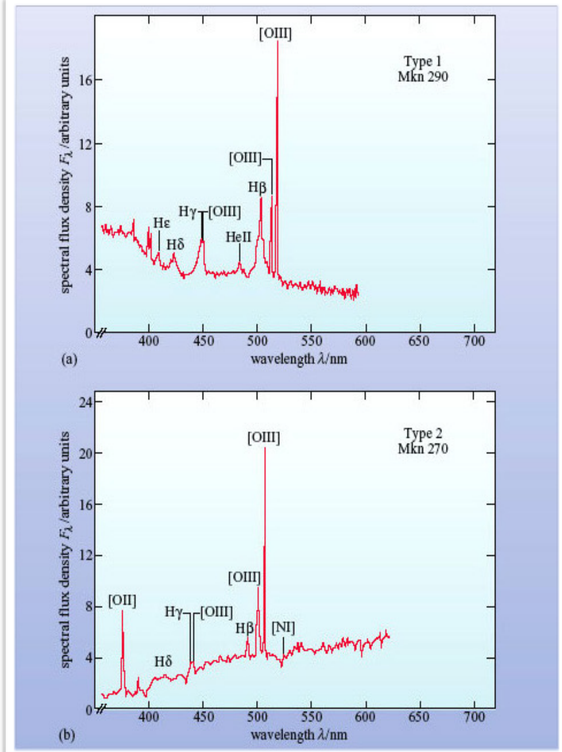

Narrow-line (Type 2) AGN

Typically, weak continuum (the disc emission is largely suppressed because of extinction), significant host-galaxy contribution in the optical, narrow permitted emission lines (several hundred km/s)

LINERs

Typically, weak continuum, dominant emission from the host galaxy, strong low-ionization emission lines (e.g., $[OI]_{6300A}$), $[OIII]/H\beta<3$ (>3 in Type 2 AGN)

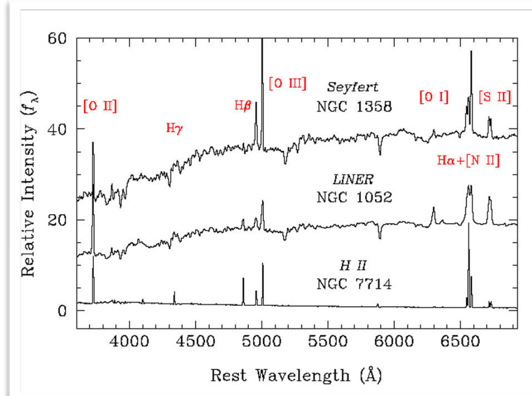

AGN optical classification. II

RL (jetted) AGN follow a similar classification as RQ AGN

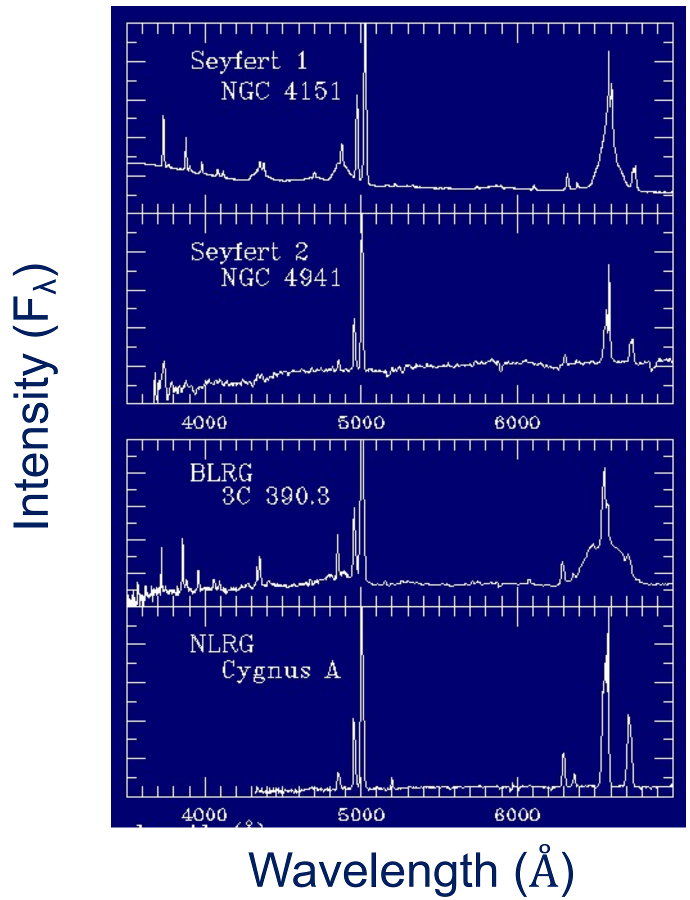

Radio-quiet (Type 1 and Type 2)

Radio-loud (Type 1 and Type 2, i.e., BLRG and NLRG)

New optical classification for RL AGN. I

Linking emission-line ratios (related to the NLR) to the efficiency of the engine

$$EI = log([OIII]/H\beta) - \frac{1}{3}\left[log([NII]/H\alpha) + log([SII]/H\alpha) + log([OI]/H\alpha)\right]$$

EI>0.95: High-Excitation Radio Galaxies (HERGs)
EI<0.95: Low-Excitation Radio Galaxies (LERGs)

Buttiglione et al. (2010)
Best & Heckman (2012)

Previously: EW([OIII]>3Å as HERGs (Laing et al. 1994)

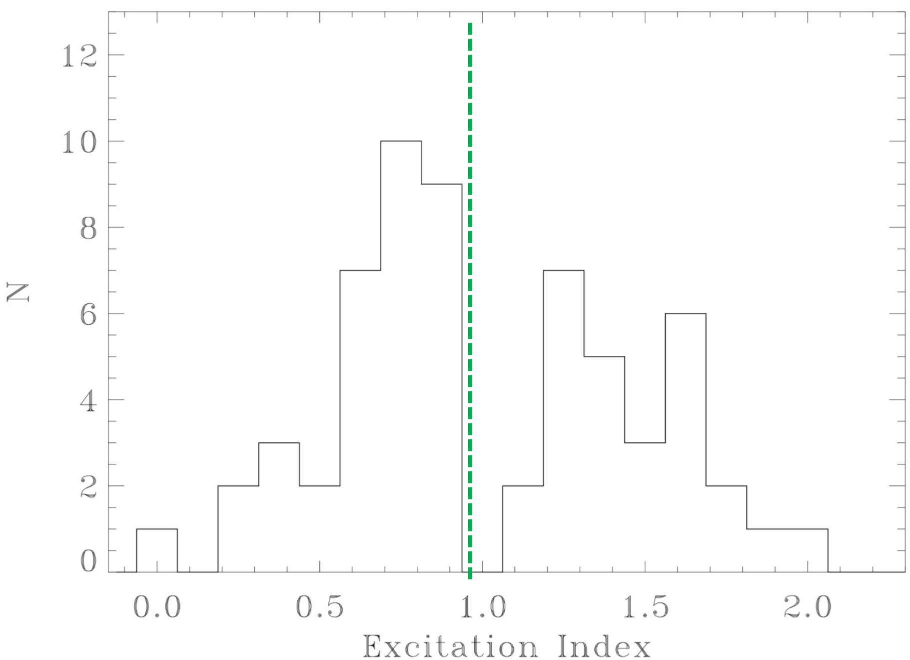

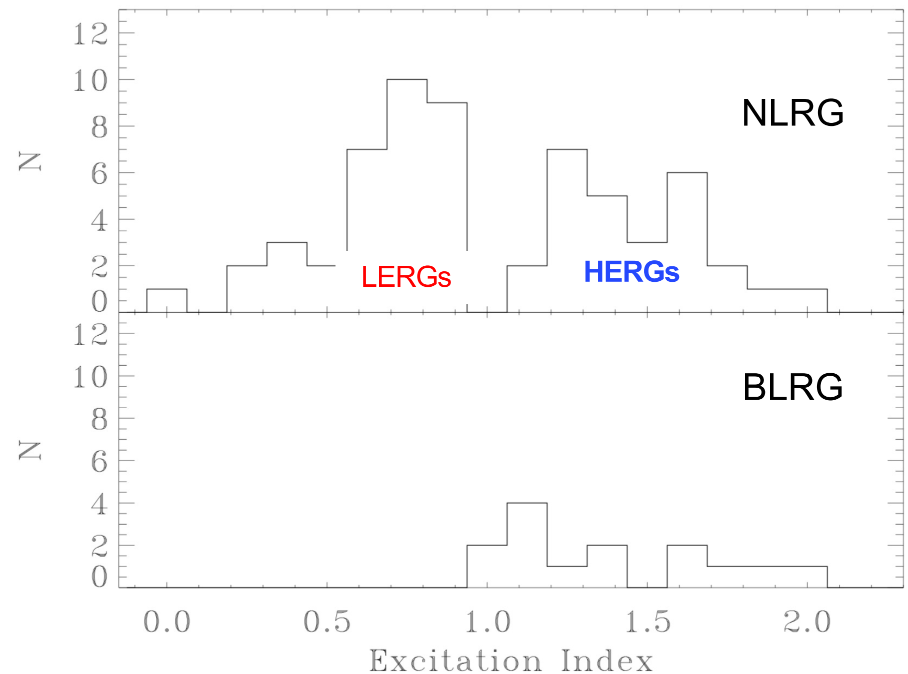

Buttiglione et al. (2010)

New optical classification for RL AGN. II

BPT diagnostic diagrams

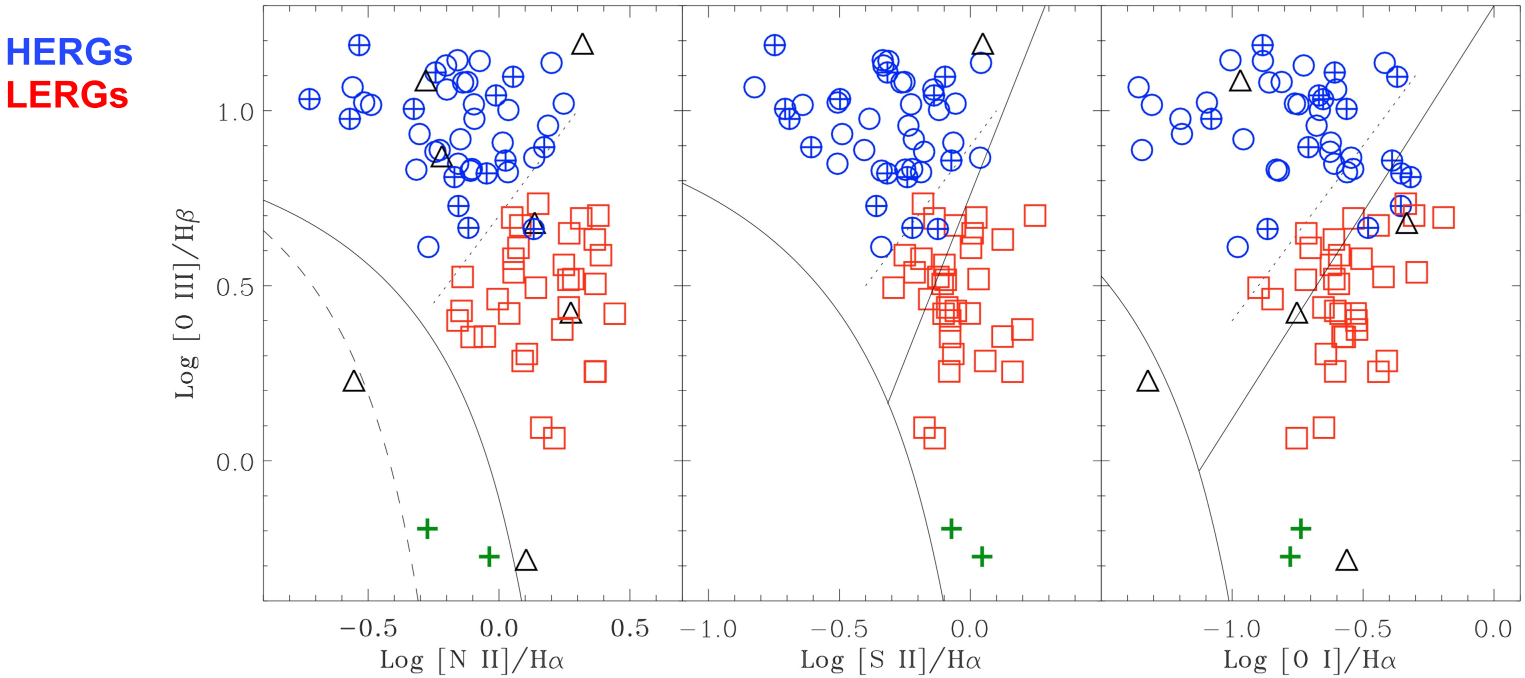

Buttiglione et al. (2010)

New optical classification for RL AGN. III

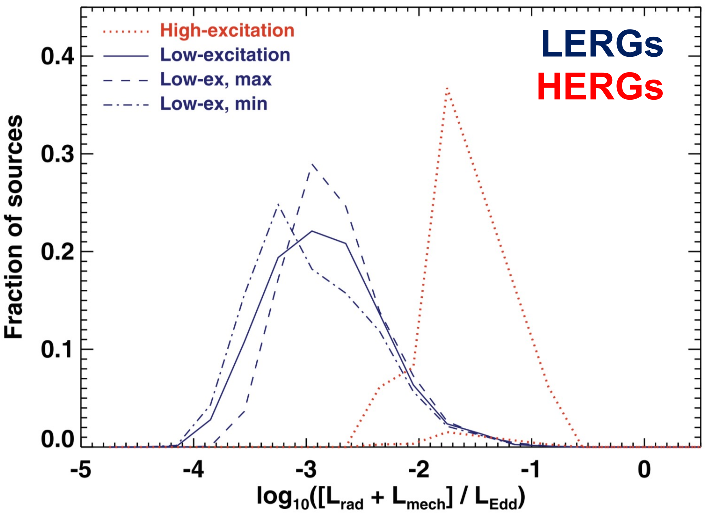

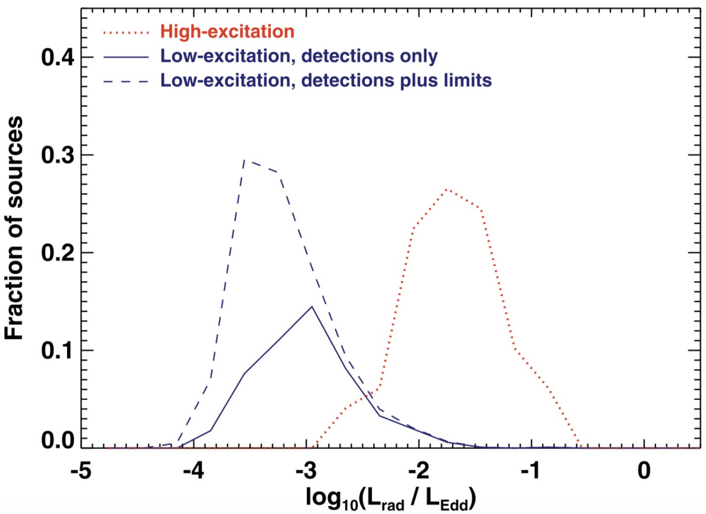

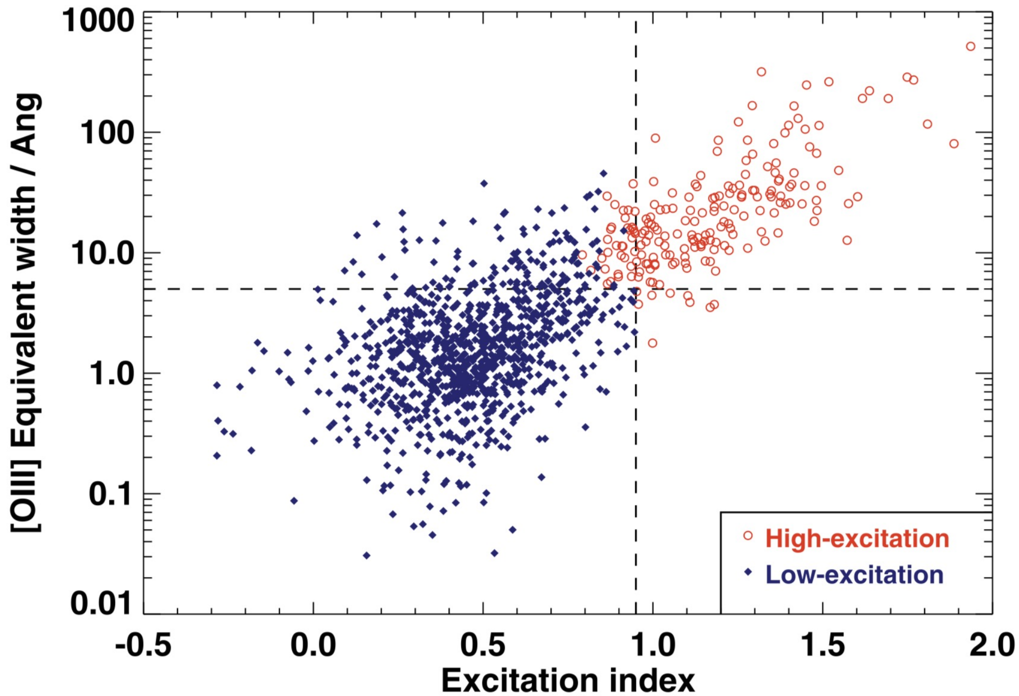

Best & Heckman (2012)

New optical classification for RL AGN. IV

HERGs: efficient engine ('standard' Shakura Sunyaev 1973 - SS73 - disc)

LERGs: inefficient engine (ADAF)

QUASAR MODE: large amounts of gas flow inwards, feeding the BH hole through a radiatively efficient SS73 disc. This mode may have a role in reducing star formation at high-redshift and setting up the observed M_{BH}-M_{bulge} relation through radiative feedback

RADIO MODE: the material is accreted onto the BH in a radiatively inefficiently way, leading to limited radiation. The bulk of energy is kinetic through radio jets (mechanical feedback, bubbles and cavities often observed)

Further insights in the accretion disc lesson

Abbr.	Meaning	Ref
NLRG	Narrow-line radio galaxy	1
BLRG	Broad-line radio galaxy	2
WLRG	Weak-line radio galaxy	3
SLRG	Strong-line radio galaxy	4
Quasar	Quasi-stellar radio source	5
LEG	Low-excitation galaxy	6
HEG	High-excitation galaxy	6
ELEG	Extreme low-excitation galaxy	6
BLRQ/Q	Broad-line radio galaxy or quasar	7
BLO	Broad-line object	6
OVV	Optically violently variable (quasar)	8
FRI	Fanaroff-Riley class I source	9
FRII	Fanaroff-Riley class II source	9
FR0	Fanaroff-Riley class 0 source	10
FSRQ	Flat-spectrum radio-loud quasar	11
SSRQ	Steep-spectrum radio-loud quasar	11
CSS	Compact steep spectrum radio source	12
GPS	Gigahertz-peaked radio source	13
FD	Fat-double radio source	14
RD	Relaxed-double radio source	15

Optical

Radio

Table 2 Summary of the main abbreviations of the labels used to classify radio AGN. The top half of the table relates to optical classifications, while the lower half relates to radio classifications. The final column gives references to some of the first uses of the labels. Reference key: 1. Costero & Osterbrock (1977); 2. Osterbrock, Koski & Philips (1976); 3. Tadhunter et al. (1998); 4. Dicken et al. (2014); 5. Schmidt (1963); 5. Buttiglione et al. (2010); 7. Dicken et al. (2009); 8. Penston & Cannon (1971); 9. Fanaroff & Riley (1974); 10. Ghisellini (2011); 11. Urry & Padovani (1995); 12. Fanti et al. (1990); 13. O'Dea, Baum & Stanghellini (1991); 14. Owen & Laing (1989); 15. (Leahy, 1993). Note that LEGs and HEGs are sometimes labelled LERGs (low excitation radio galaxies) and HERGs (high excitation radio galaxies) in the literature.

Tadhunter (2016); see also Padovani et al. (2017 review)

FRI vs. FRII classification: source morphology. I

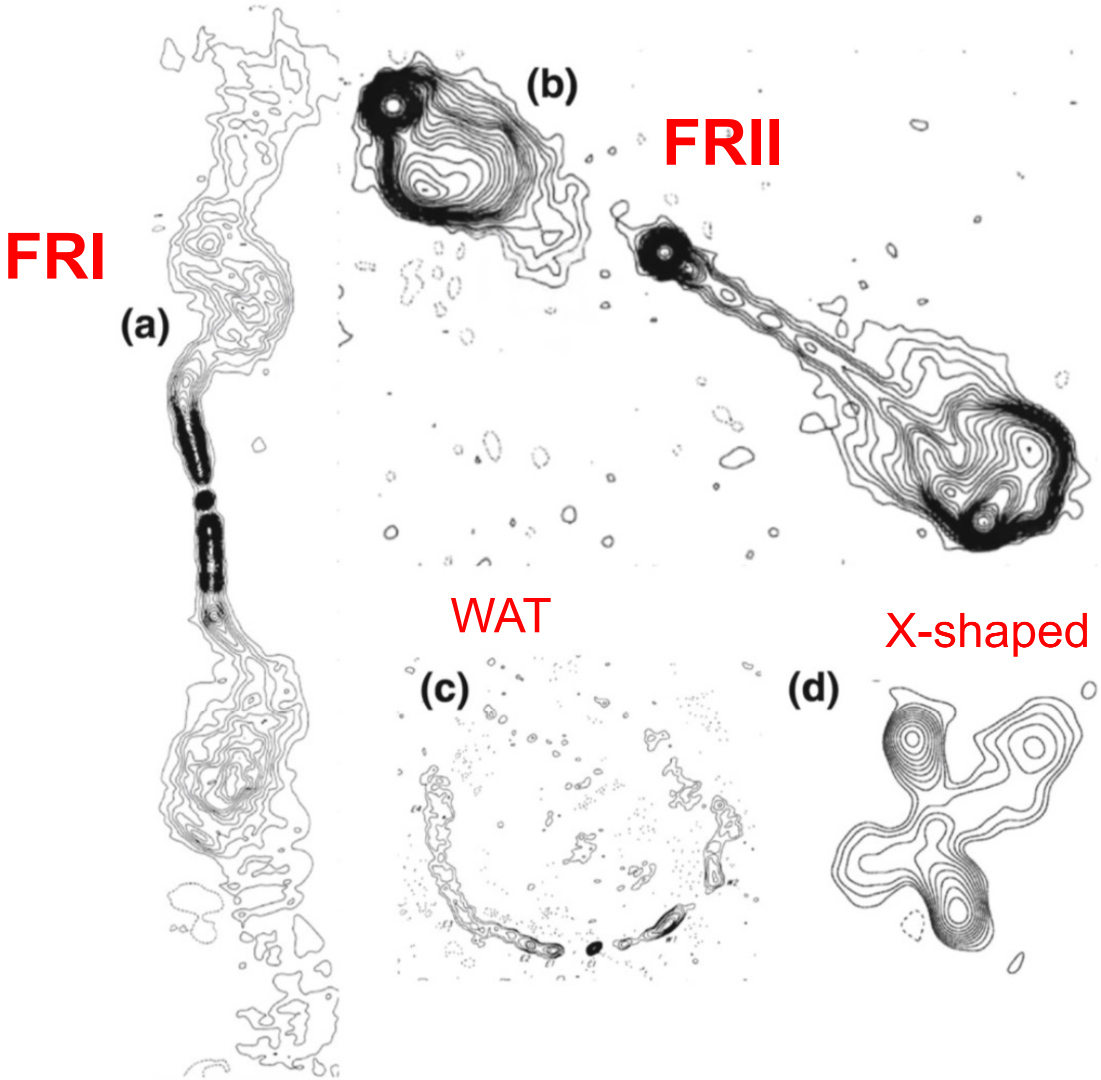

Radio galaxies have different morphologies. Main classification include **FRI** and **FRII** (Fanaroff & Riley 1974)

Environment and mergers have a role in shaping radio galaxies

WAT: wide-angle tail
NAT: narrow-angle tail
HT: head tail

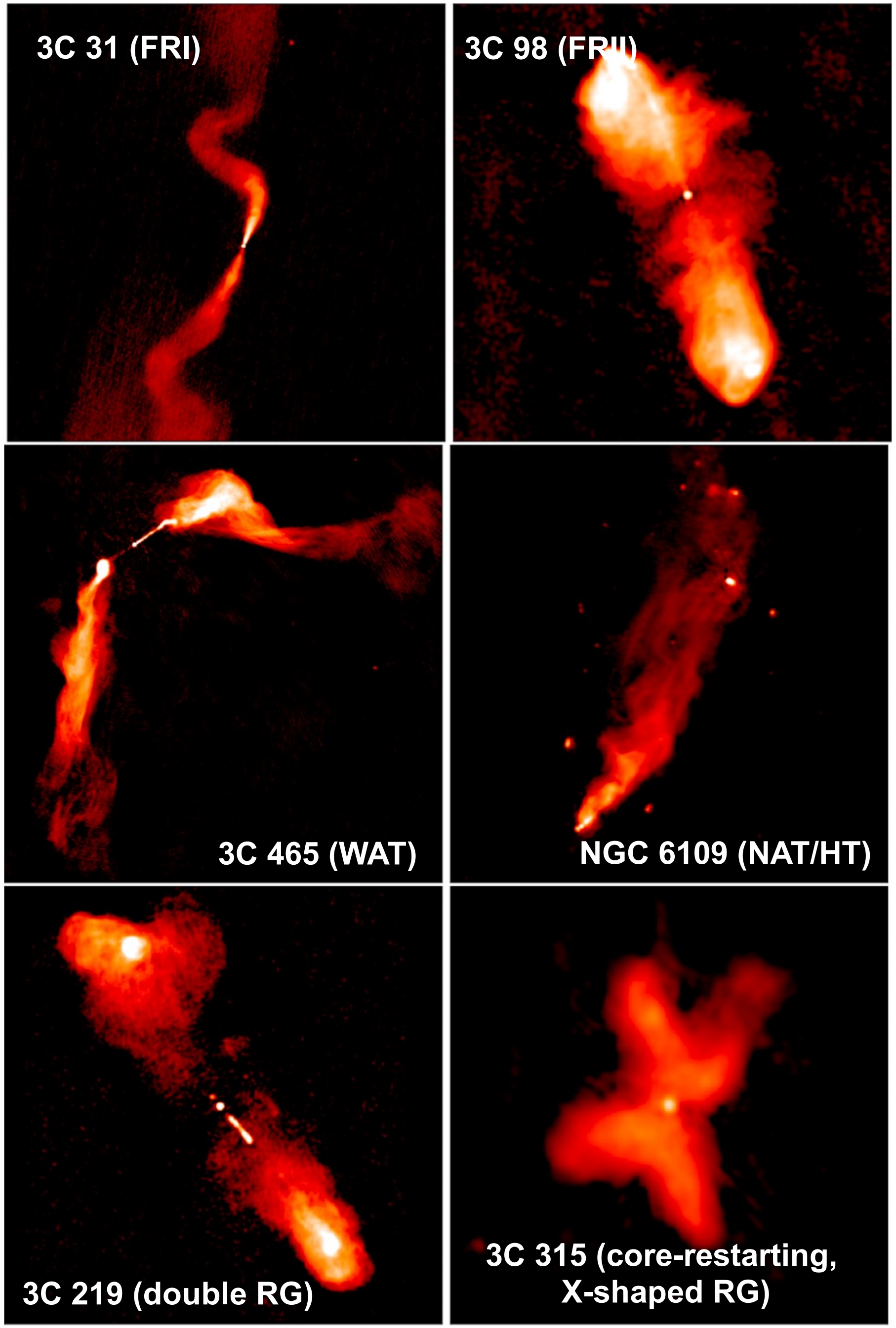

Hardcastle & Croston
(2020 review)

FRI vs. FRII classification: source morphology. II

R=ratio of the separation of the highest surface brightness regions on opposite sides of the central galaxy and the extent of the source measured from the lowest surface brightness contour

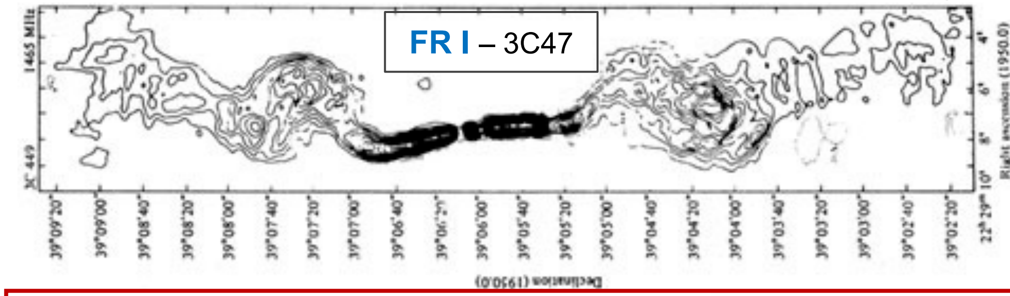

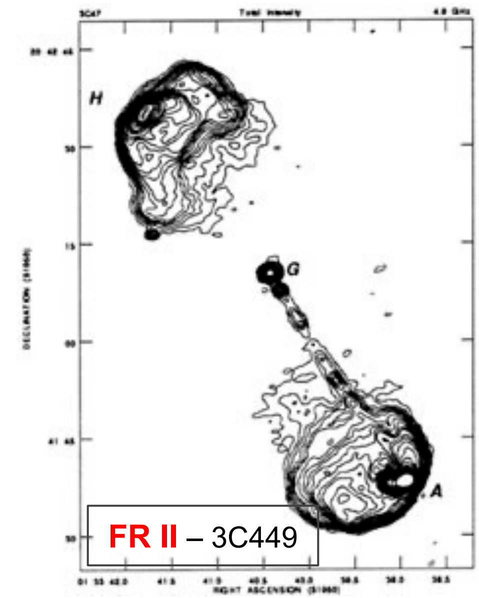

- **FRI**: R<0.5
- $L_{178MHz} \lesssim 10^{25}$ W/Hz/ster
- Dominated by the compact core and the jets (2-sided) Diffuse lobes in the outer regions fading with distance
- Parent population of BL Lacs?

- **FRII**: R>0.5
- $L_{178MHz} \gtrsim 10^{25}$ W/Hz/ster
- Radio lobes dominate over 1-sided jet (Doppler boosting of approaching jet and deboosting of receding jet) − swept-back material or backflow from the shocked region due to the advance of the head of the jet. Hot spots coincident with the location of the working surface of the beam
- Typically, in poorer environments
- Parent population of FSRQs?

FRI vs. FRII classification: source morphology. III

Extended radio structures well beyond the size of the host galaxy
→ possible feedback up to Mpc scales

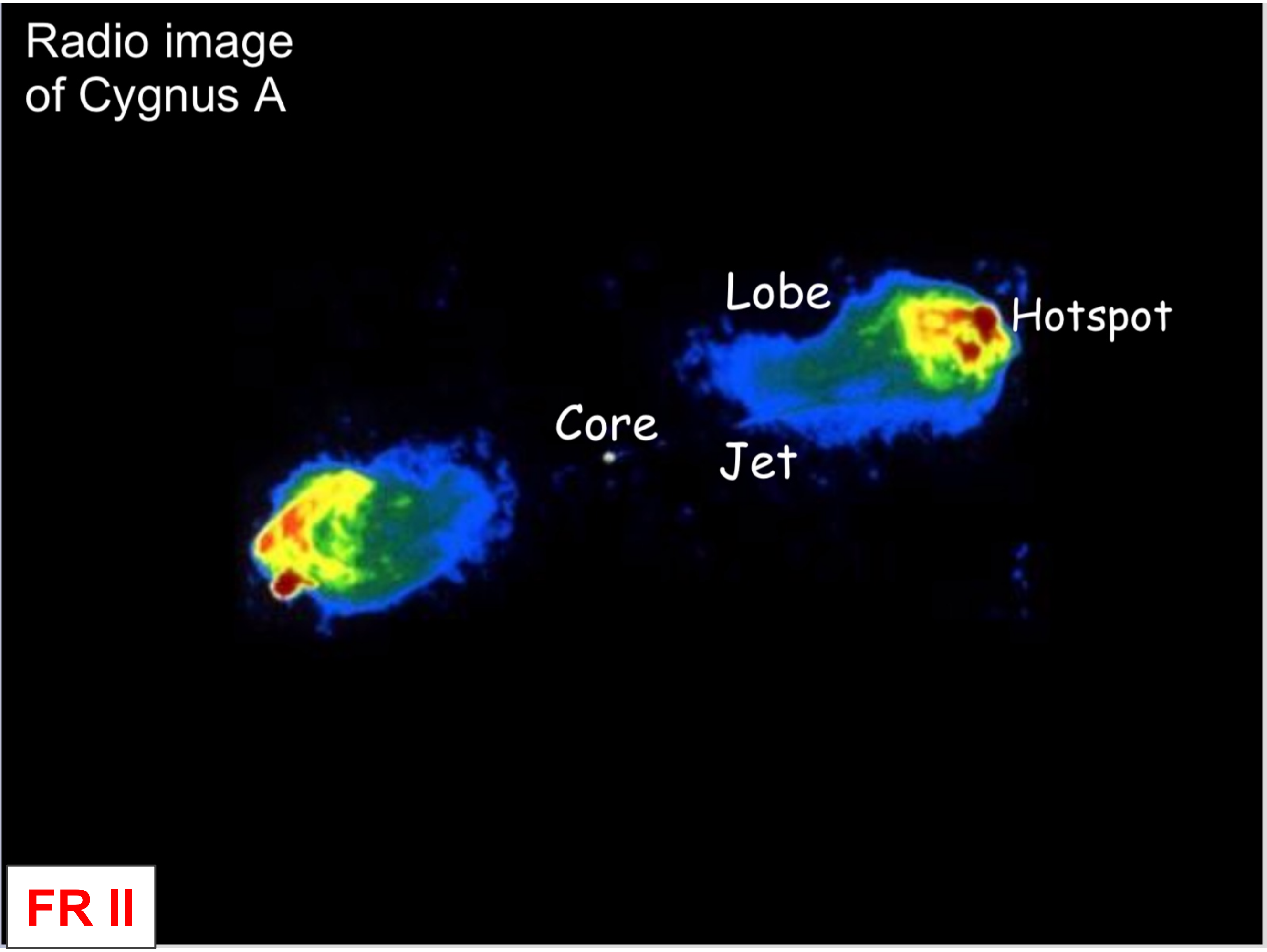

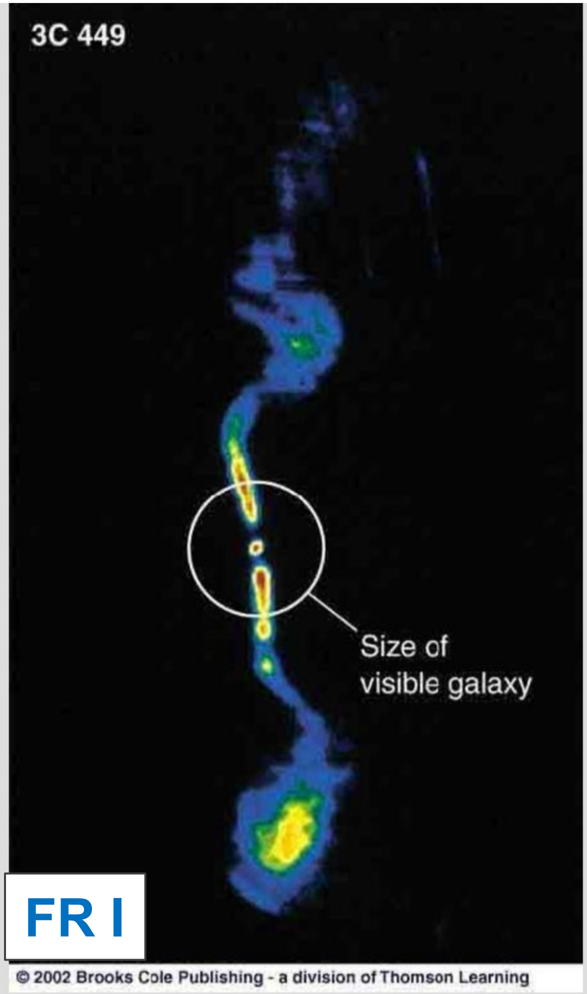

FRI vs. FRII classification: source morphology. IV

FRI are referred to as jet-dominated and *edge-darkened*

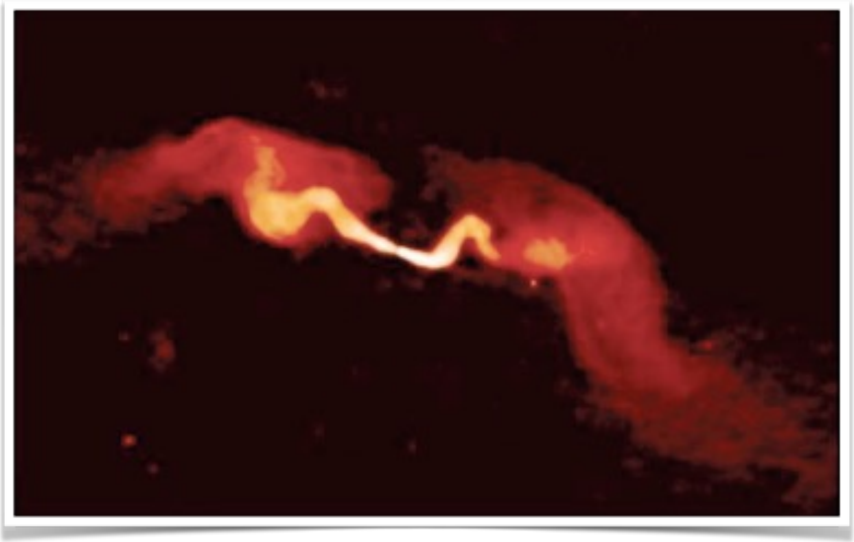

In **FRI** the jets are though to be decelerated and become sub-relativistic on scales of hundred of pc to kpc
Their nuclei are powered by an **inefficient engine**

FRII are referred to as lobe-dominated and *edge-brightened*

In **FRII** the jets are at least moderately relativistic and supersonic from the core to the hot spots
Most of their nuclei are powered by an **efficient engine**

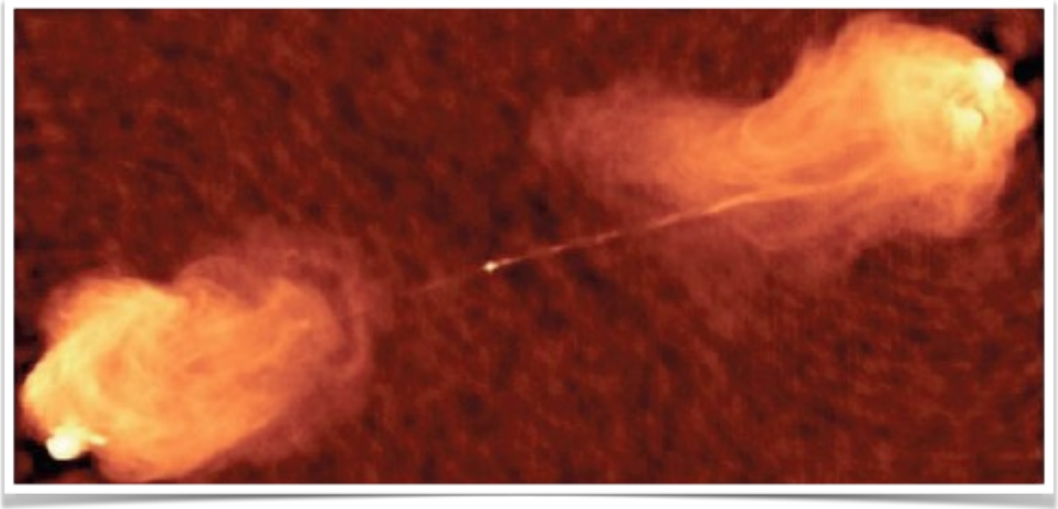

FRI vs. FRII classification: source morphology. V

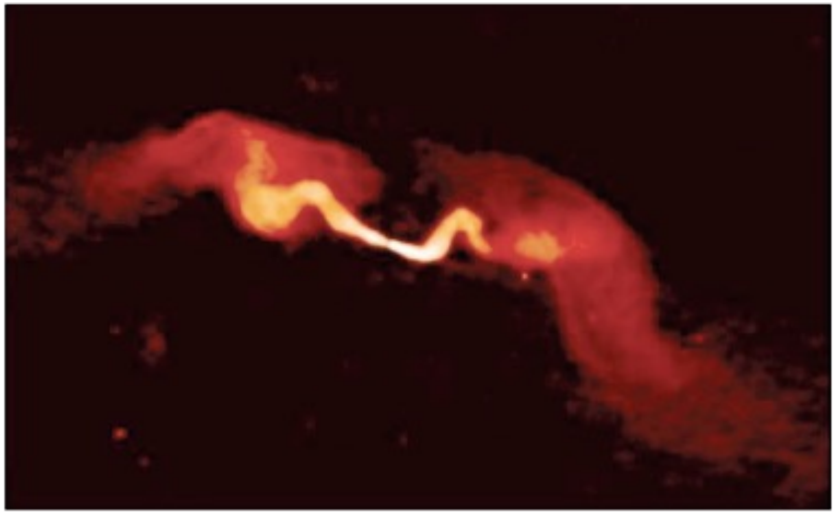

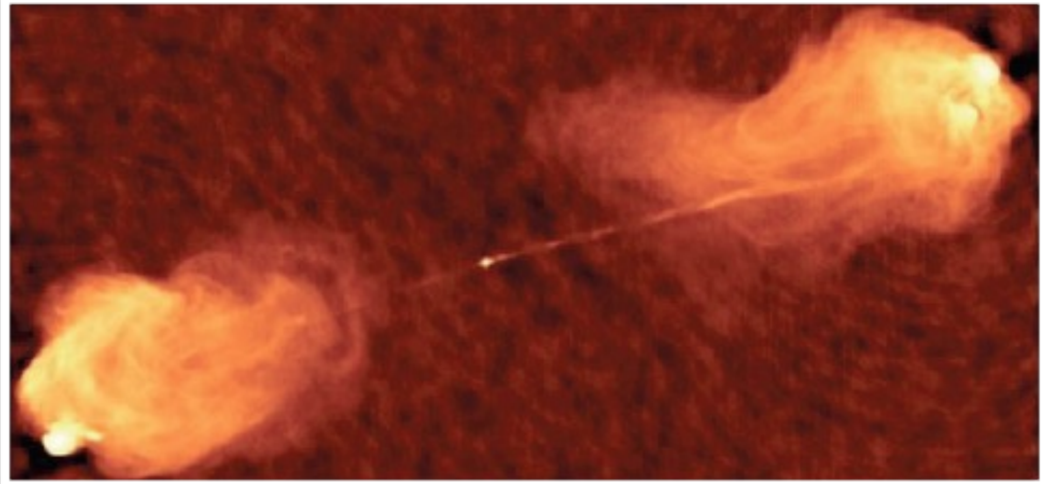

FRI = LERG

FRII = HERG (mostly)

Different engine: ADAF vs. standard (efficient) accretion disc

Jets. I

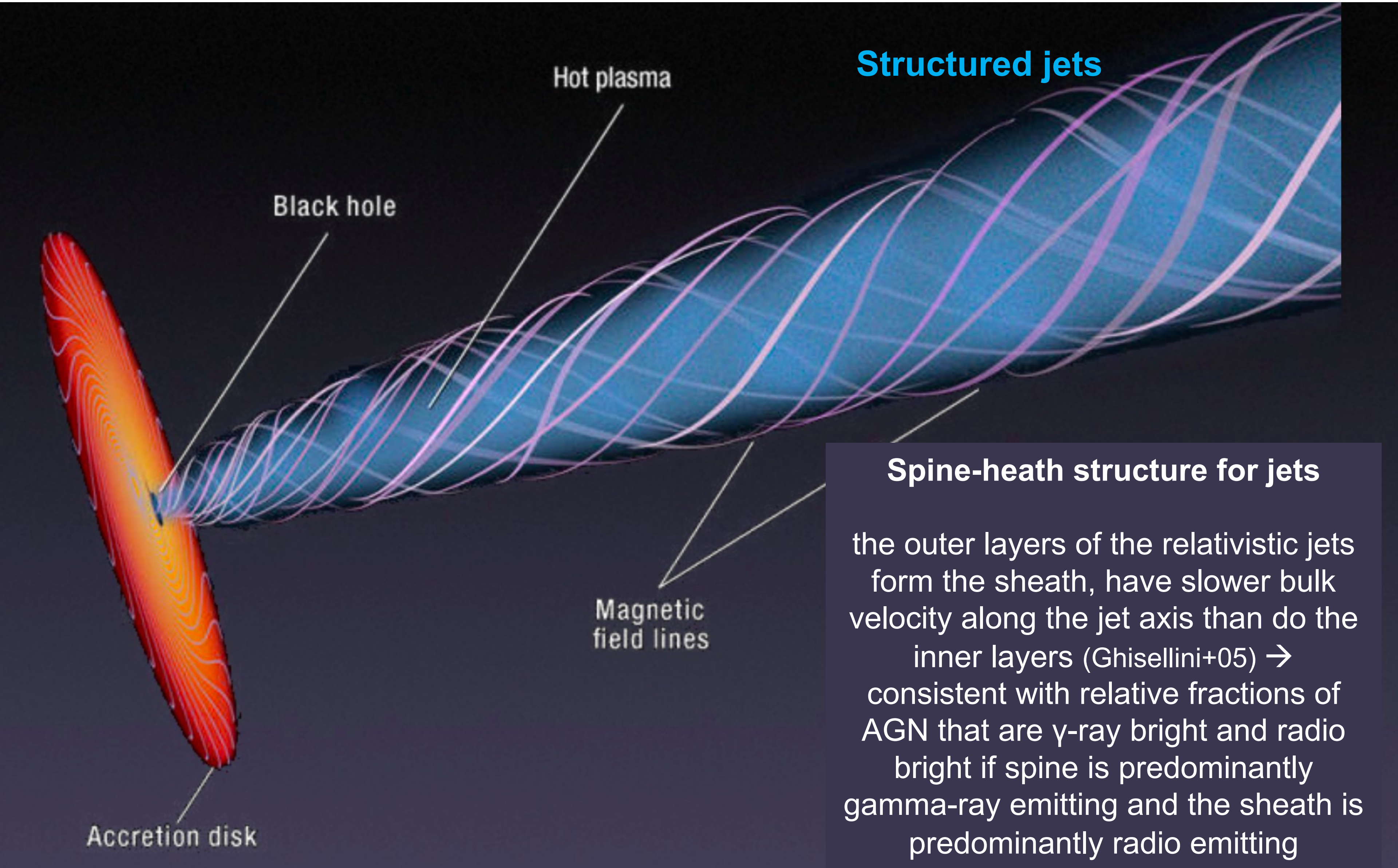

Spine-heath structure for jets

the outer layers of the relativistic jets form the sheath, have slower bulk velocity along the jet axis than do the inner layers (Ghisellini+05) → consistent with relative fractions of AGN that are γ-ray bright and radio bright if spine is predominantly gamma-ray emitting and the sheath is predominantly radio emitting

Jets. II

Deceleration in jets
entrainment of external gas
(FRI jets more prone to
this effect; Bicknell 1994)

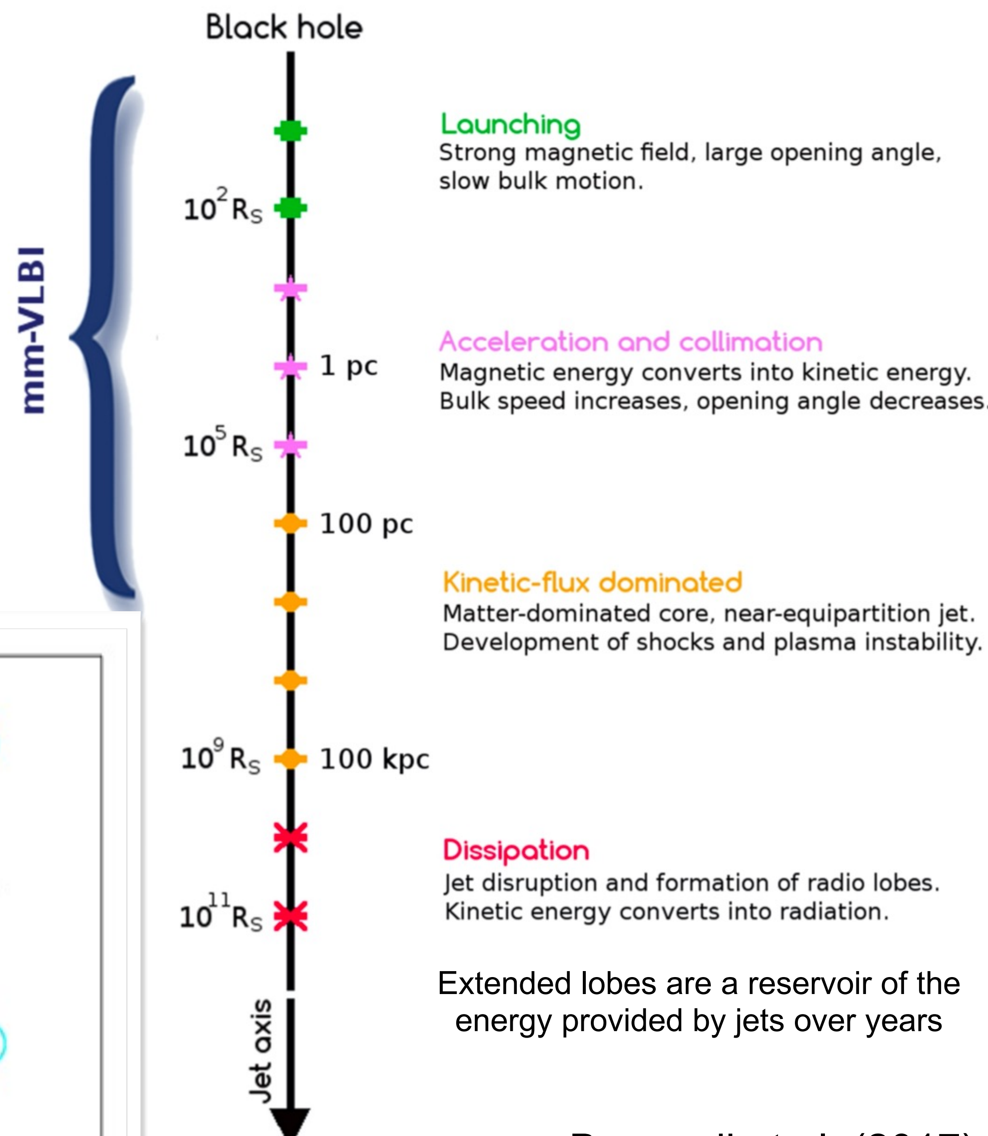

Extended lobes are a reservoir of the energy provided by jets over years

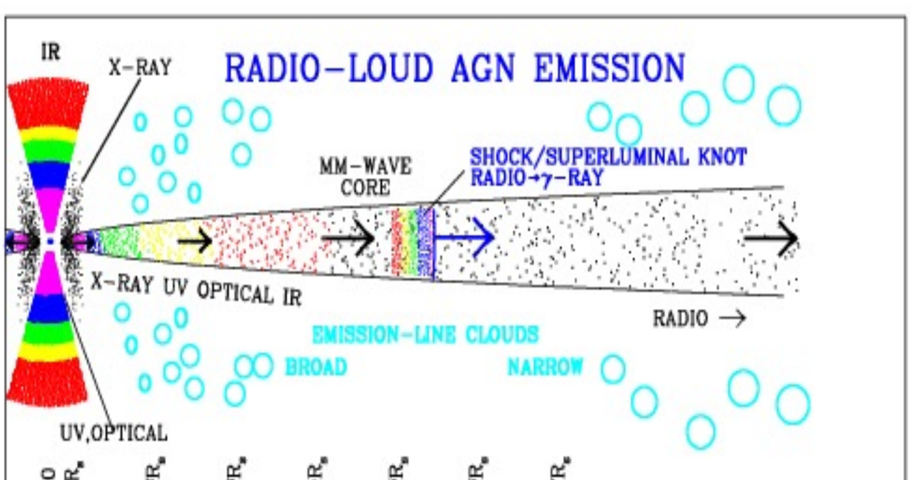

Courtesy of Marscher

Boccardi et al. (2017)

Jets. III

Jet base studies require high angular resolution and reduced synchrotron + free-free opacity → mm band to probe acceleration and collimation

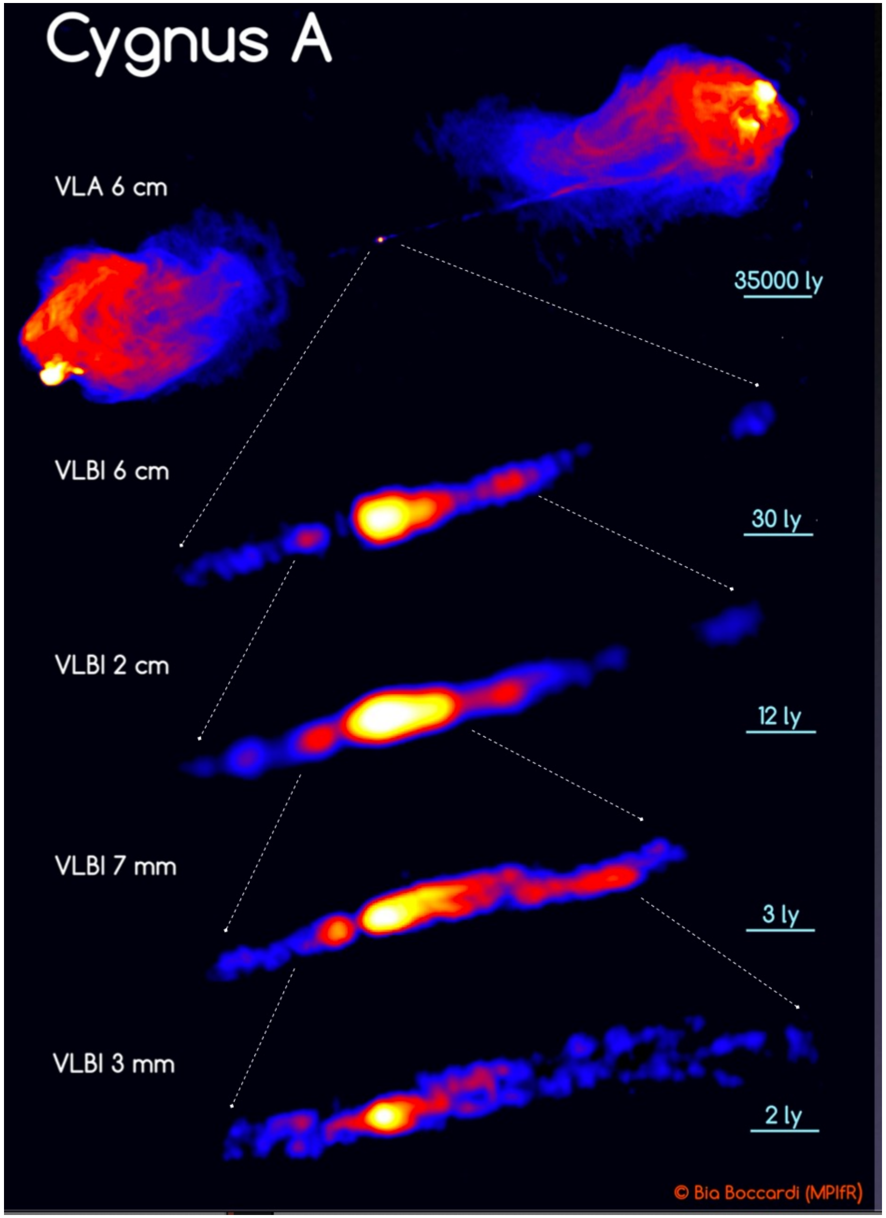

Boccardi et al. (2017)

Jets. IV

Jet Formation and properties: some considerations

Relativistic jets form when the *BH spins* and the *accretion disc* is *strongly magnetized*. AGN jets are collimated close to the BH by magnetic stress associated with a disc wind (produced by magnetic instabilities at the surface of the disc, giving rise to flares, hence a wind)
The twisting of the magnetic field lines, tied to the rotation of the BH, can lead to *highly collimated jets*

Their power relies either on the gravitational energy of accreting matter onto the BH (Blandford & Payne 1982) and/or by the *Blandford-Znajek* (1977) *process* (see also Penrose 1969), i.e. *extraction of rotational energy from the rotating BH*: the accreting material transports the magnetic field down to the event horizon where it can be twisted by the rotation of space-time close to the BH
In other words, *the work done in generating the jet comes directly from the rotation of the BH*

Both mechanisms can generate jet powers of $\sim 10^{45\text{-}47}$ erg/s (Blandford et al. 2019) → $E \sim 10^{59\text{-}61}$ erg into lobes (assuming $t \sim 10^7$ yrs)
$U_{pot,grav}$ is transformed into heat and radiation and can also amplify the magnetic field, allowing the field to access the large store of BH E_{rot} and transform part of it into $E_{mech,jet}$ (Ghisellini et al. 2014)

Link of radio activity with stellar mass (above $\sim 10^{11}$ $M_\odot$ to have power jets)?
'Underlying' relation with halo density?

Still many open issues in jet formation and theory vs. observations

Jets. V

Ω and B are the main parameters

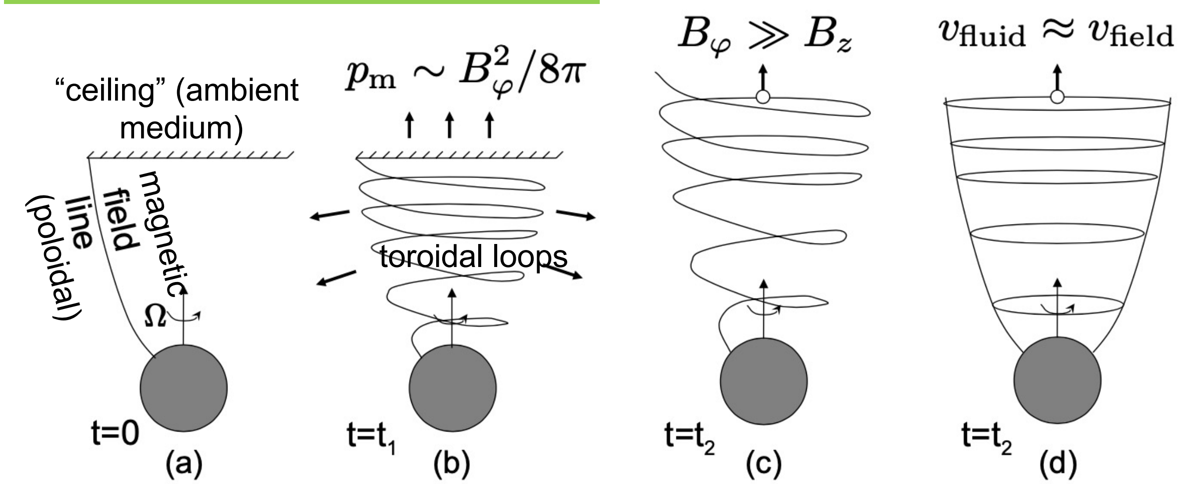

Slices of the vertical and horizonal direction
Essential role of the accretion disc

Red: high density

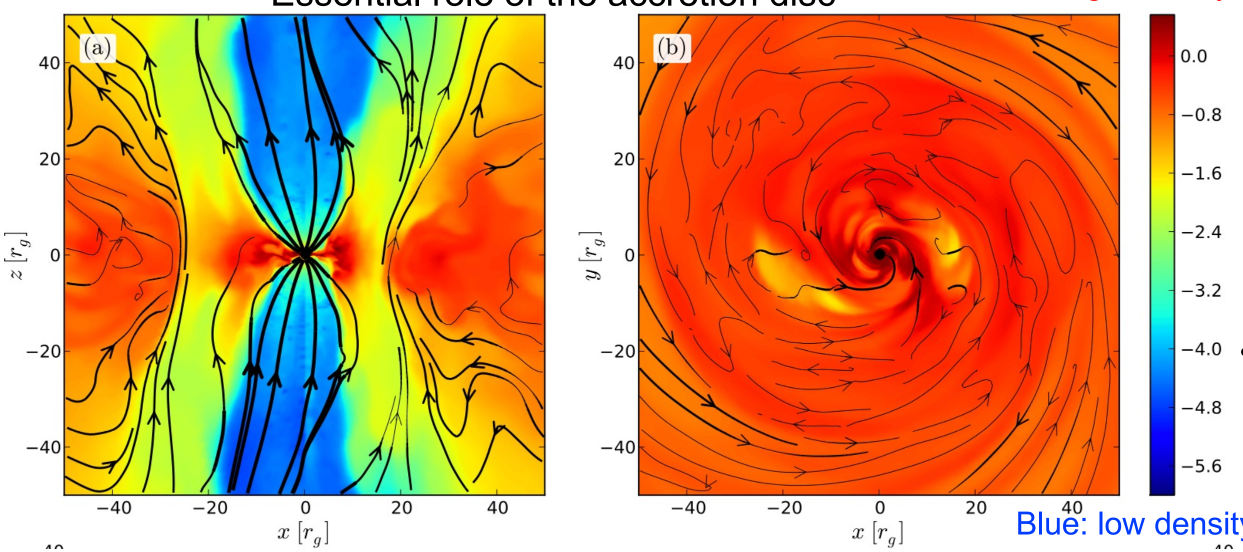

Blue: low density

Tchekhovskoy+12; see also MartÍ 2019 and Davis & Tchekhovskoy 2029 reviews

- Magnetic field anchored to the accretion disc (spinning BH) and to a stationary, perfectly conducting, 'ceiling' (i.e., the ambient medium) – Panel (a).
- After N rotations, the field develops N toroidal loops. Bφ pushes the 'ceiling' with an effective pressure P_M~$B^2/8\pi$ and accelerates the plasma along the rotation axis forming a jet – Panel (b).
- The poloidal electromagnetic flux of energy (Poynting flux, PF) accelerates the magnetospheric plasma and plasma from the disc along the poloidal magnetic field lines, converting the PF into kinetic energy of bulk motion, reaching relativistic speeds at extended scales – Panel (c).
- The rotation of the BH continuously twists the poloidal field into new toroidal loops at a rate which, in steady state, balances the rate at which the loops move downstream – Panel (d).

Jets. VI

$$a = \frac{Jc}{GM^2}$$

Dimensionless spin parameter (J=angular momentum)

$$r_H = r_g \left[1 + (1 - a^2)^{1/2}\right]$$

BH horizon radius

$$\Omega_H = \frac{ac}{2r_H}$$

BH angular frequency

$$P_{BZ} = \frac{k}{4\pi c} \Phi^2_{BH} \frac{a^2}{16 r_g^2}$$

Rate of extraction of rotational energy from the BH
(Blandford & Znajek 1977)
Low-spin limit: $a^2 \ll 1$
$k \sim 0.05$; Φ_{BH}=magnetic field flux across the BH horizon

$$P_{BZ} = \frac{k}{4\pi c} \Phi^2_{BH} \Omega^2_H f(\Omega_H)$$

BZ6 formula, accurate for all *a* values
$F(\Omega_H) \sim 1 + 1.38(\Omega_H r_g/c)^2 - 9.2(\Omega_H r_g/c)^4$
(Tchekhovskoy et al. 2012)

Jets. VII

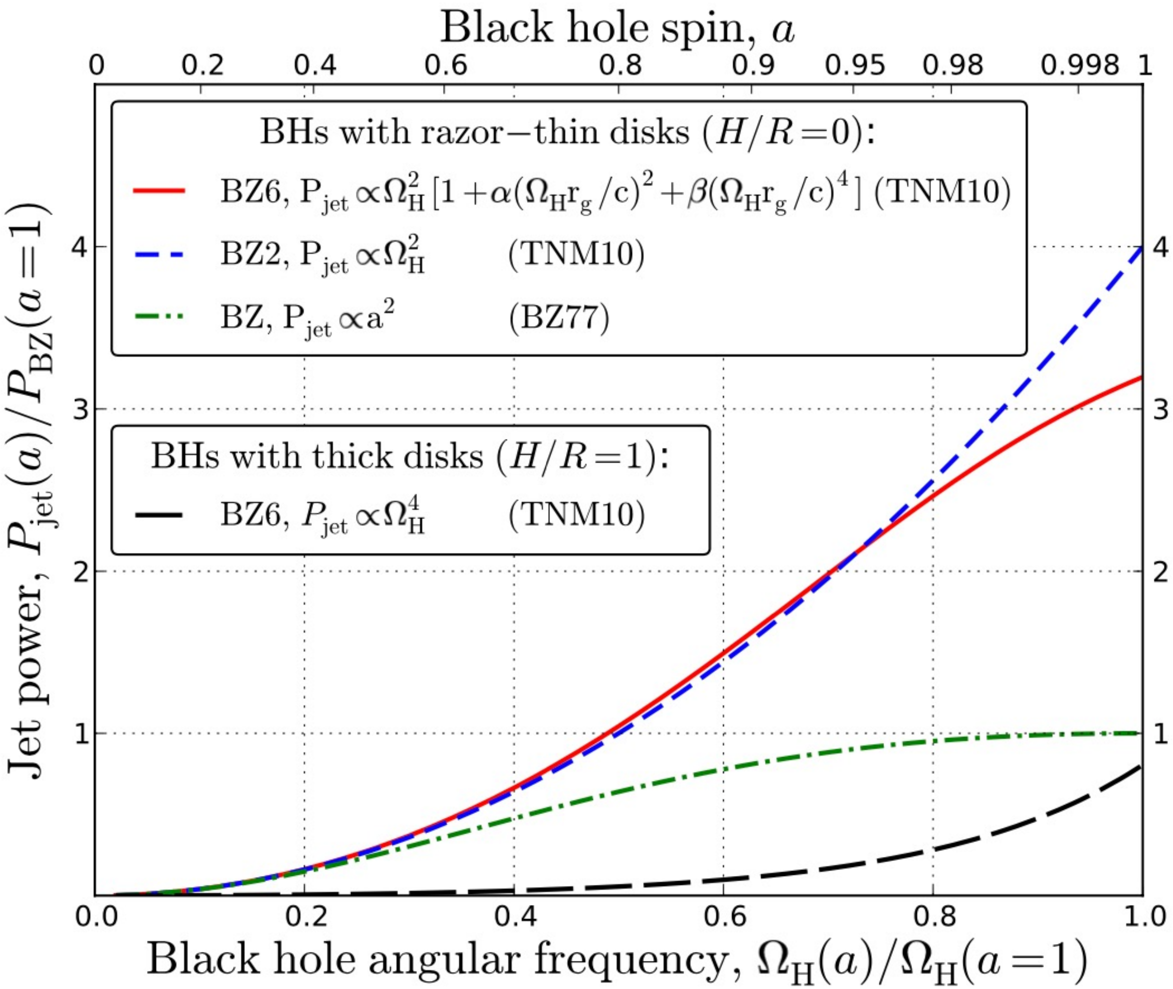

P_{jet} vs. BH angular frequency (both normalized to maximum achievable power from BZ77 original solution - green curve). *The standard BZ77 solution remains accurate up to a~0.3*; *for maximally rotating BHs it under-predicts P_{jet} by a factor ~3* (wrt. BZ6 solution).

In case of **thick discs**, P_{jet} has a stronger dependence on the BH angular frequency → *high BH spins significantly enhance the possibility of having AGN with high radio-loudness parameters* (factors x100−x1000 higher in RL AGN than in RQ AGN)

Tchekhovskoy+12

Jets. VIII

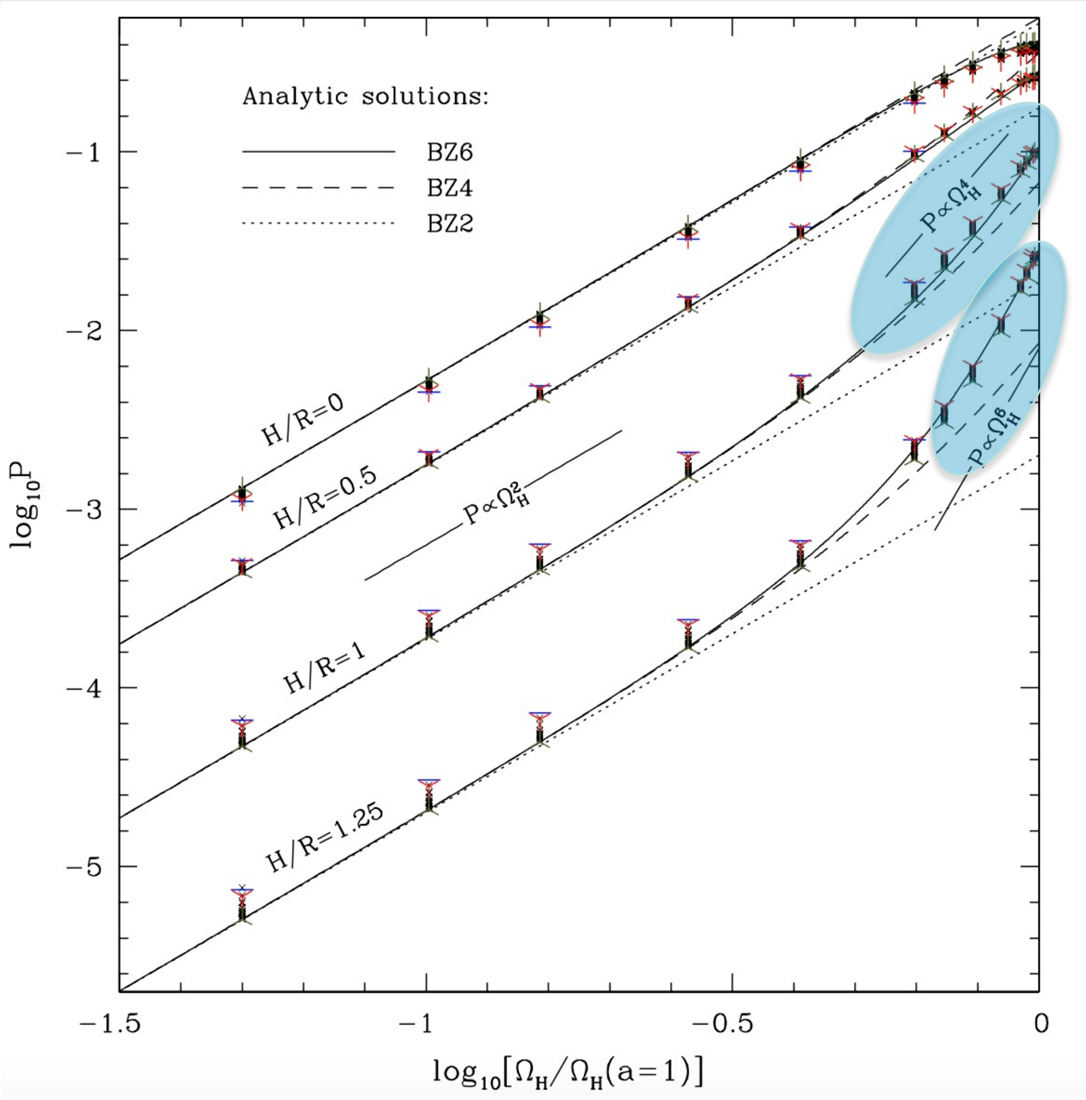

Tchekhovskoy+10; see also McKinney05

When a BH is surrounded by a thick disc/corona, equatorial field lines from the BH at lower latitudes pass through the disc/corona, become turbulent and produce a slow baryon-rich wind, whereas polar field lines at higher latitudes lie away from the disc gas and produce a Poynting-dominated relativistic jet (McKinney 2005)

$\mathbf{P_{jet} \propto \Omega^4_H}$ (even Ω^6_H for very thick discs)

Changes in the solid angles subtended by the jet (via changes in the disc thickness) could change the steepness of P_{jet} as a function of *a*.

The different spin distribution of RQ and RL AGN may reflect different accretion and mergers histories of SMBHs in spirals and ellipticals

Jets. IX

Strongly Doppler-boosted radiation in jets

$$\delta(\beta,\theta) = \frac{1}{\gamma(1-\beta cos\theta)}$$

Doppler factor

ϑ angle between the jet axis and the line of sight

$$\beta = \frac{v}{c}$$

$$\gamma = \frac{1}{\sqrt{1-\beta^2}}$$

Lorentz factor

The Doppler factor relates intrinsic and observed flux for a moving source at relativistic speed v=β c

For an **intrinsic** power law spectrum: $F'(\nu') = K\,(\nu')^{-\alpha}$
the **observed** flux density is

$$F_\nu(\nu) = \delta^{3+\alpha}\, F'_{\nu'}(\nu)$$

$$\Delta t = \Delta t'/\delta$$

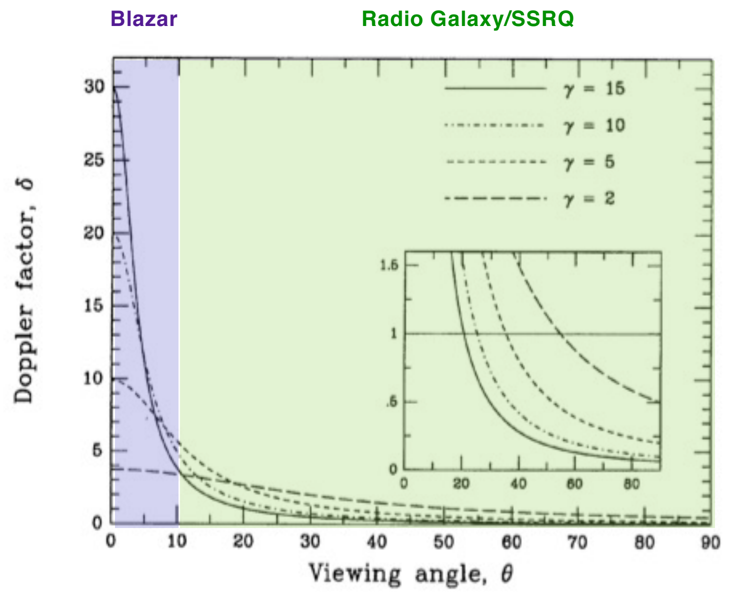

Small angles: blazars. I

BL LAC
No/weak lines in the optical spectrum (featureless continuum)

Flat spectrum radio quasars (FSRQ)
Can show emission lines overimposed on a strong continuum

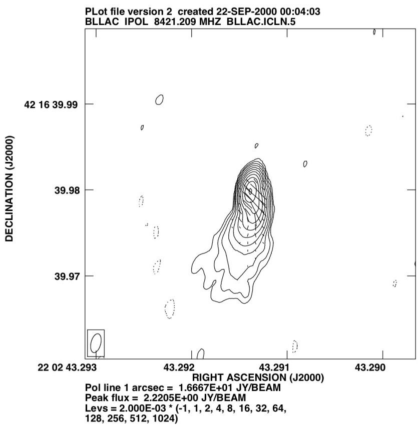

Both classes are compact in radio images

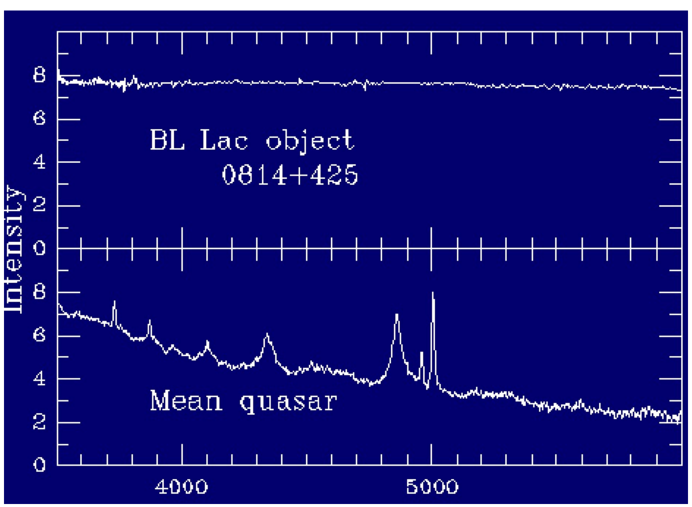

BL LACs are almost featureless

Both classes are extremely variable at all frequencies

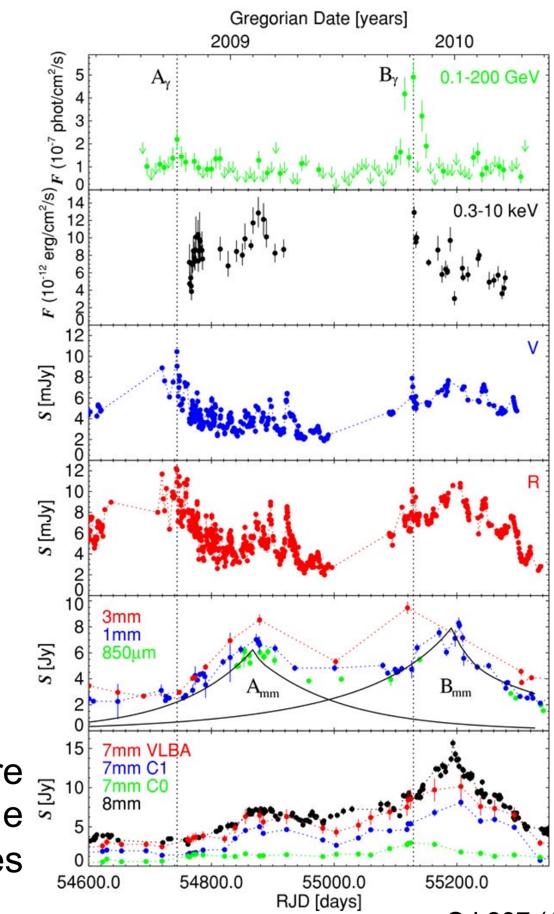

OJ 287 (Agudo et al. 2011)

Blazars. II

Towards a revision of the Unified model for jetted AGN

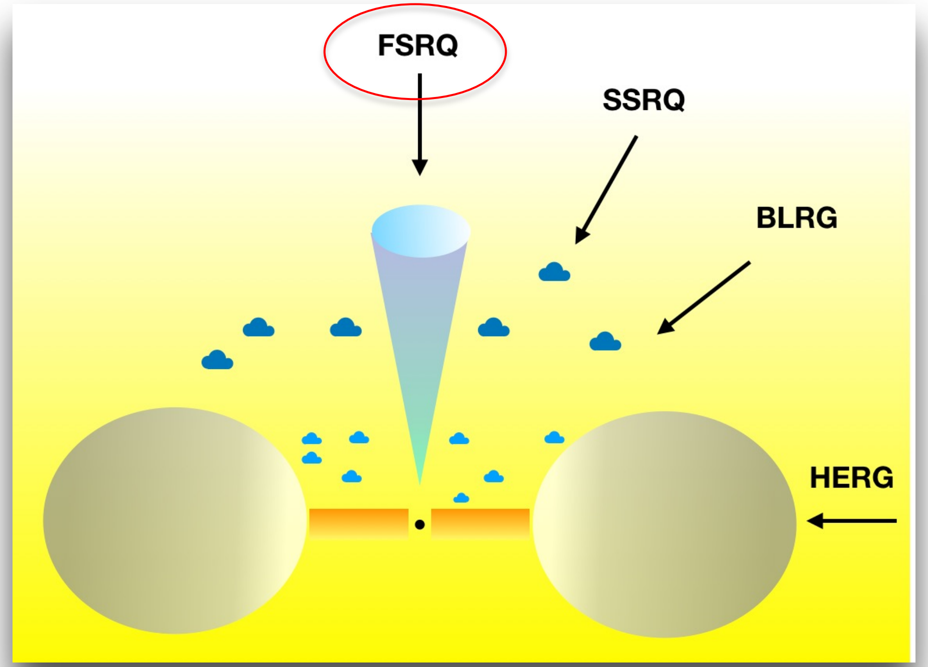

FSRQs: efficient accretion = stardard disc

BL Lacs: inefficient accretion flow = ADAF solution

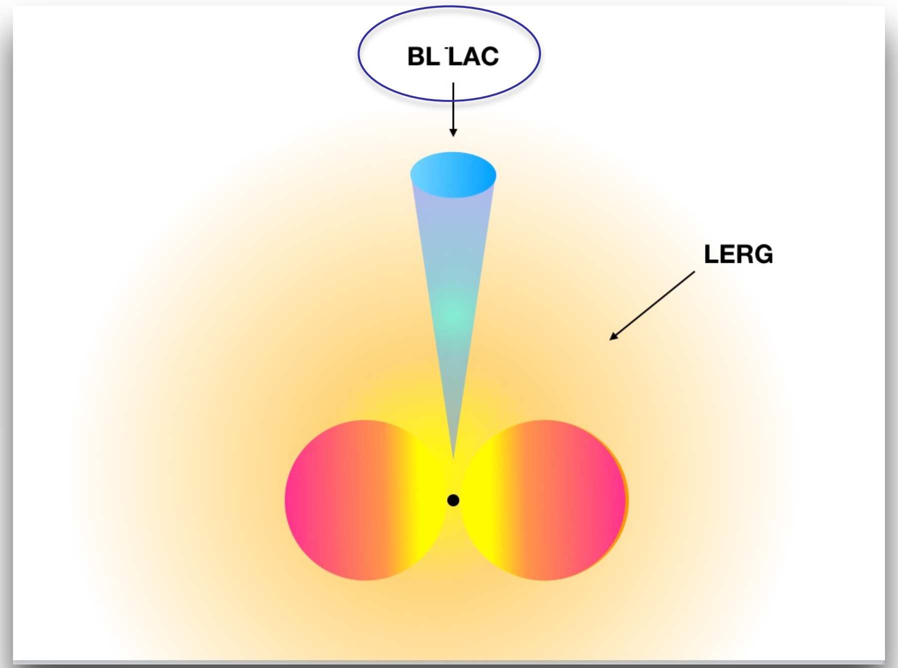

The overall “picture”. I

Inclination angle wrt the jet

Radio Galaxies HERG

Blazar

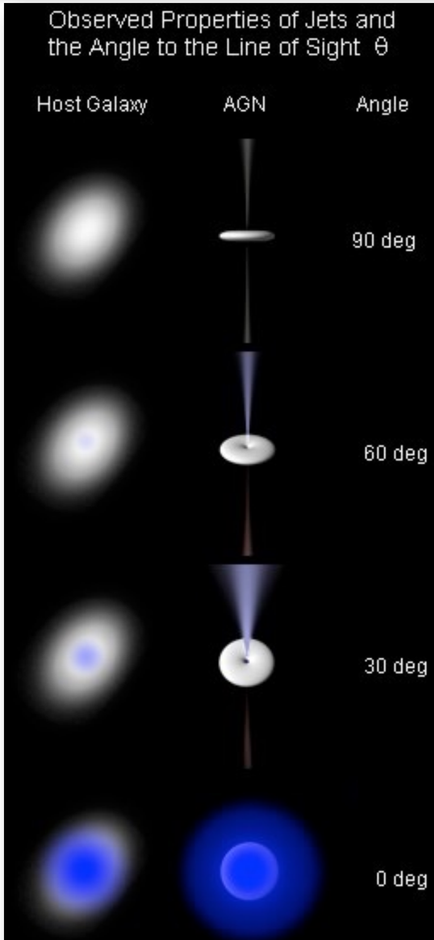

NLRG (Type 2)

BLRG (Type 1)

HERG: thermal radiation dominates the spectrum in the IR/optical/UV/X-ray

In HERG spectra, accretion disc and jet emission are in competition

Angle~0 deg: jet radiation dominates
Angle~90 deg: accretion disc dominates

HERG (BLRG): thermal and non thermal radiation are ‘rival’

BLAZAR: non-thermal radiation dominates throughout the spectrum

LERG: non-thermal radiation dominates the spectrum (inefficient accretion flow)

The overall “picture”. II

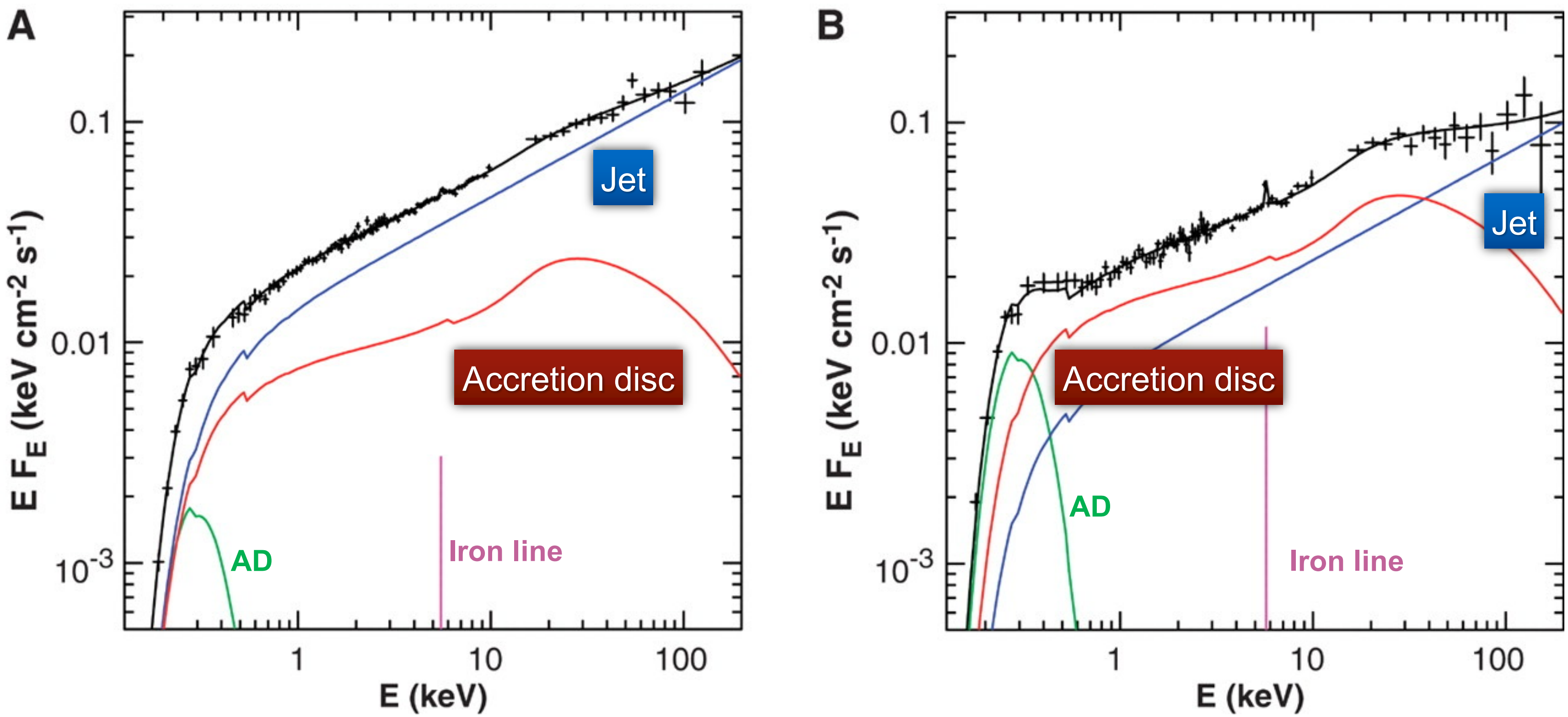

3C273 (FSRQ): generally, the spectrum in this FSRQ at small inclination angle is dominated by the jet (**A**). However, when the jet is less bright, the accretion disc (including the IC emission due to the primary AGN emission) and the iron line emerge (**B**, as in radio-quiet sources)

Courtesy of P. Grandi

The overall “picture”. III

3C120 (BLRG): the torus and the blue bump are evident in the SED
The X-ray spectrum shows the presence for a significant iron Kα emission line
→ looking at objects at inclination angles >> 0 deg wrt. the jet axis in RL AGN allows to observe emission properties similar to those of radio-quiet AGN (here: disc emission-Blue Bump and iron Kα emisson line)

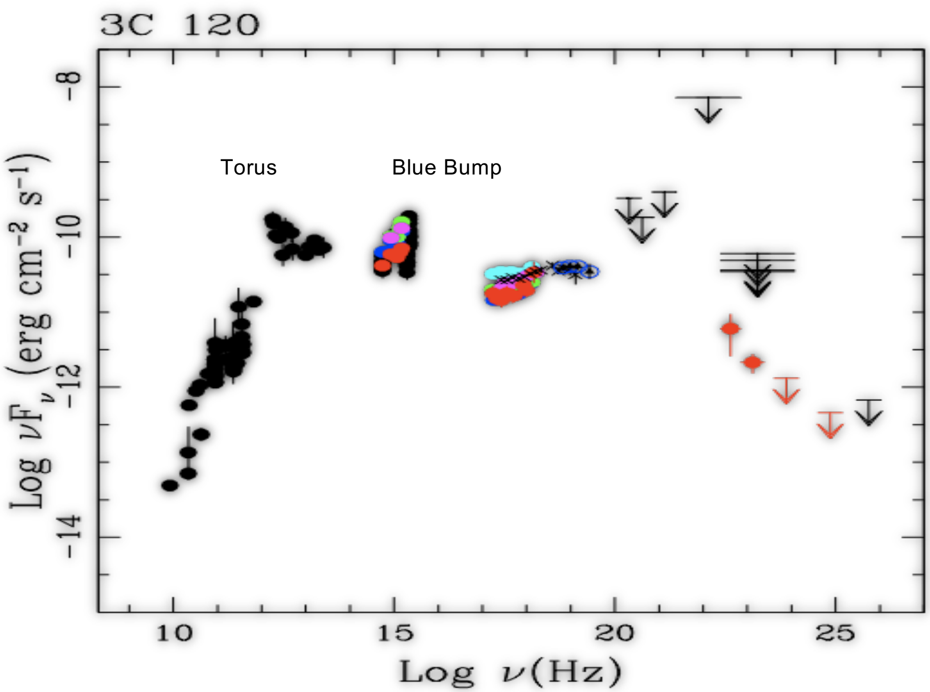

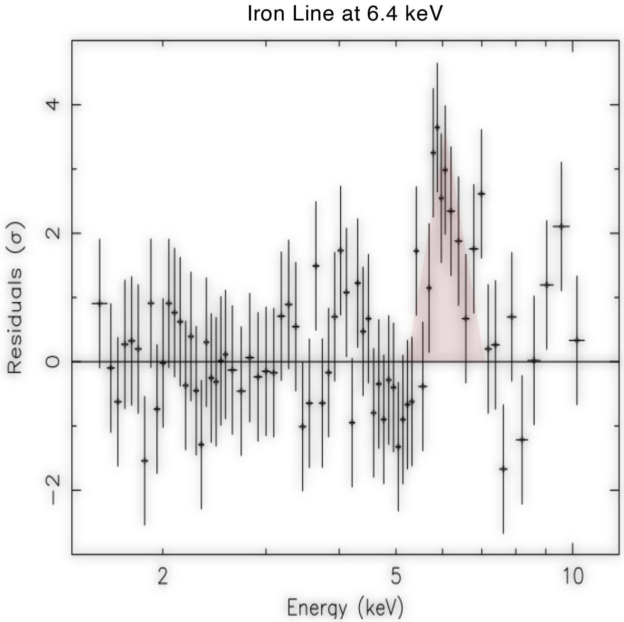

Courtesy of P. Grandi

The core emission

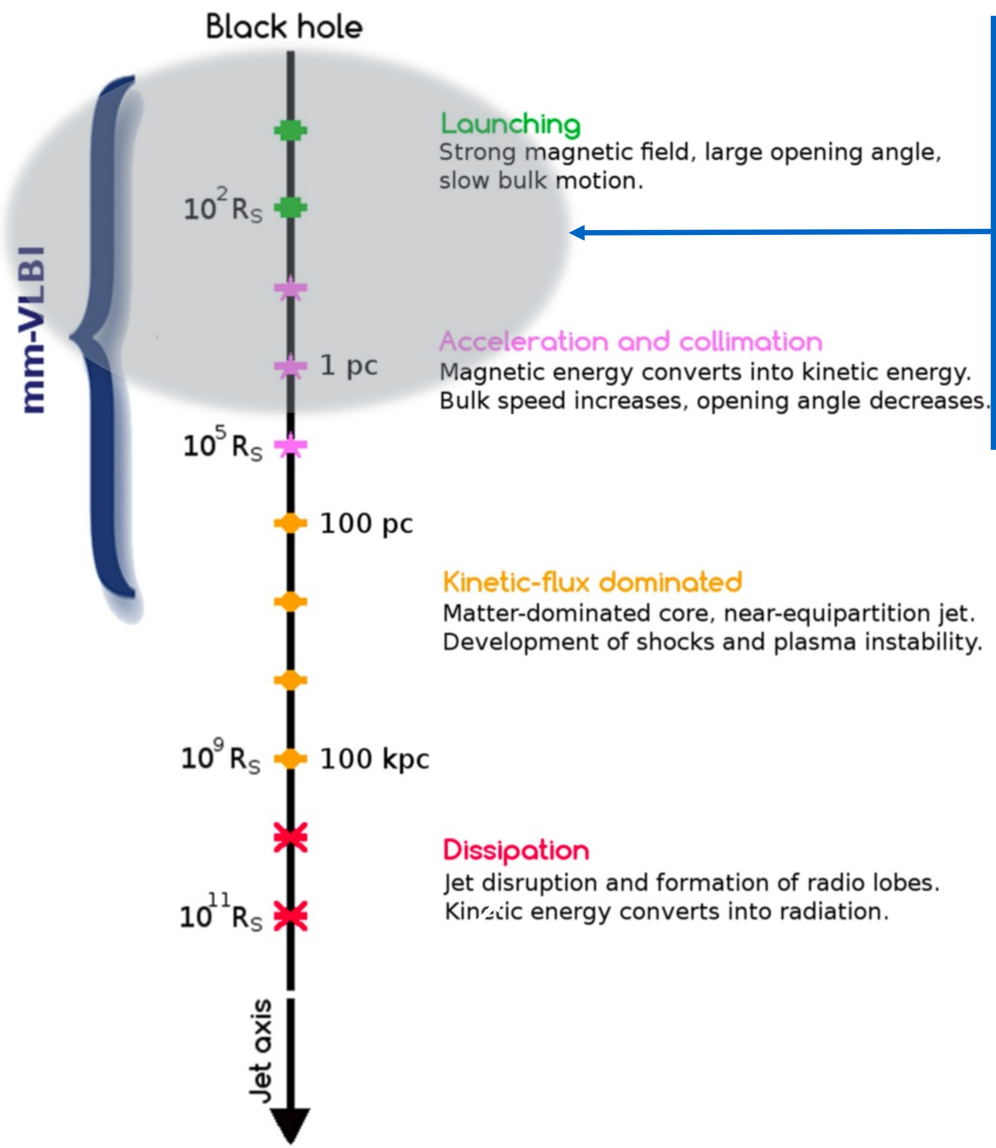

Non-thermal radiation coming from the core region dominates the SED if the jet intercepts the line of sight of the observer (blazar) and/or the accretion is inefficient (LERG)

The observed SED consists of two peaks of emission

Double-peaked SEDs.I

Product of the jets in blazars: the **blazar sequence**

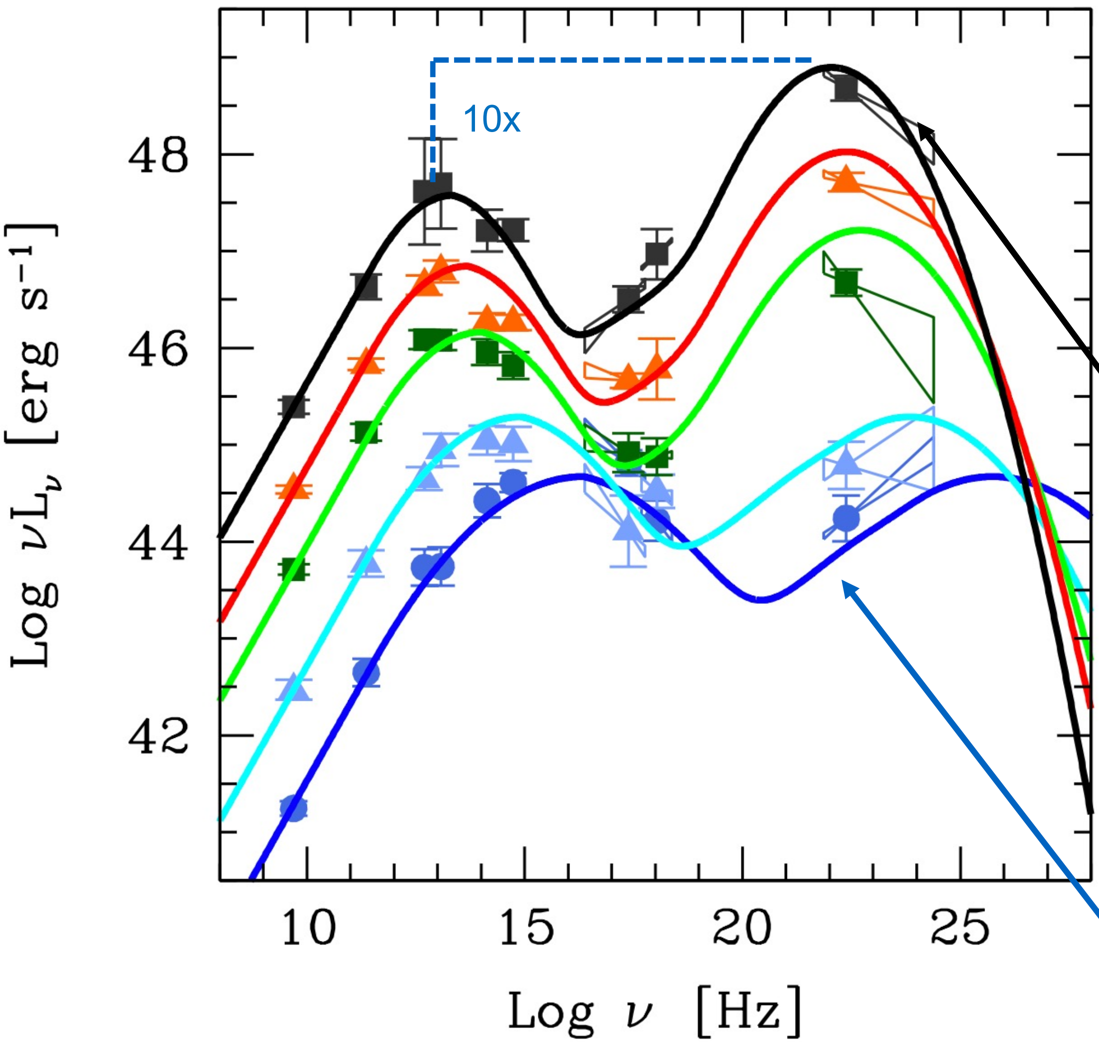

Fossati’s sequence (1998 paper)
Ghisellini et al. (2016) review

The first peak is in the IR → X-ray
The second peak is in the MeV → TeV

- High-power and strong-line blazars have radiatively efficient discs and are able to ionize the clouds of the BLR. Part of the disc luminosity is reprocessed by the torus in the IR → seed photons (produced externally to the jet) for the IC → powerful high-energy emission
- *SED is red*, peaking in the submm (synchrotron) and in the MeV (IC) bands
- The IC emission dominates over the synchrotron emission (Compton dominance)

- Low-power and lineless BL Lacs have a radiatively inefficient disc → little ionization of the BLR → fewer seed photons to be scattered at high energies
- Radiative cooling rate is weaker, allowing the electrons to reach high energies → *blue SED* (peaking at higher energies)
- Almost equal synchrotron and IC luminosities

Double-peaked SEDs.II

BL LAC

SSC (Synchrotron Self-Compton)

Relativistic electrons in a magnetized region → synchrotron → The same electrons will upscatter the synchrotron-generated photons and produce the IC peak

FSRQ

IC via external photons

Relativistic electrons in a magnetized region can also interact with photons external to the jet produced in the accretion disk, in the BLR/NLR and the torus via IC

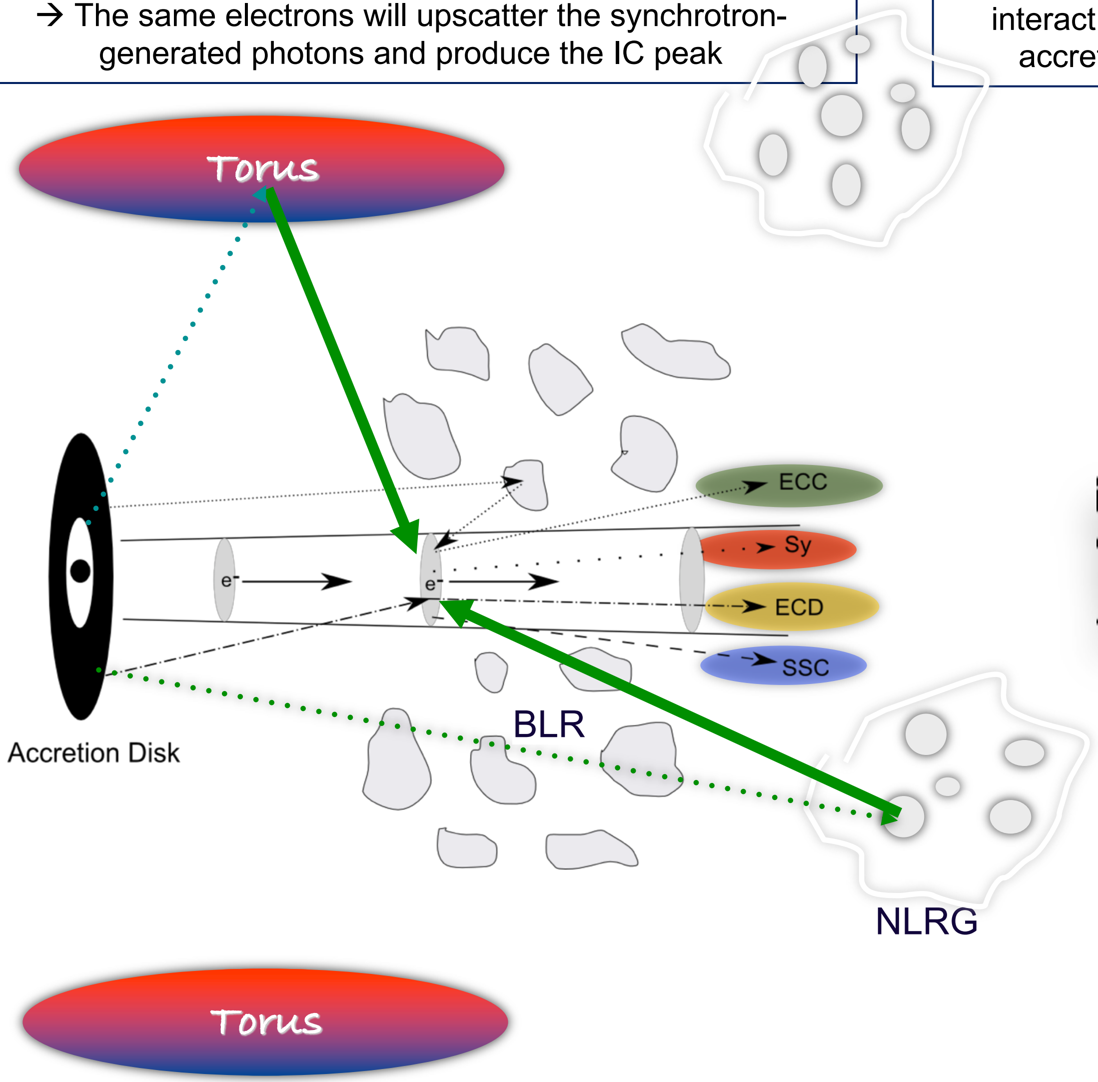

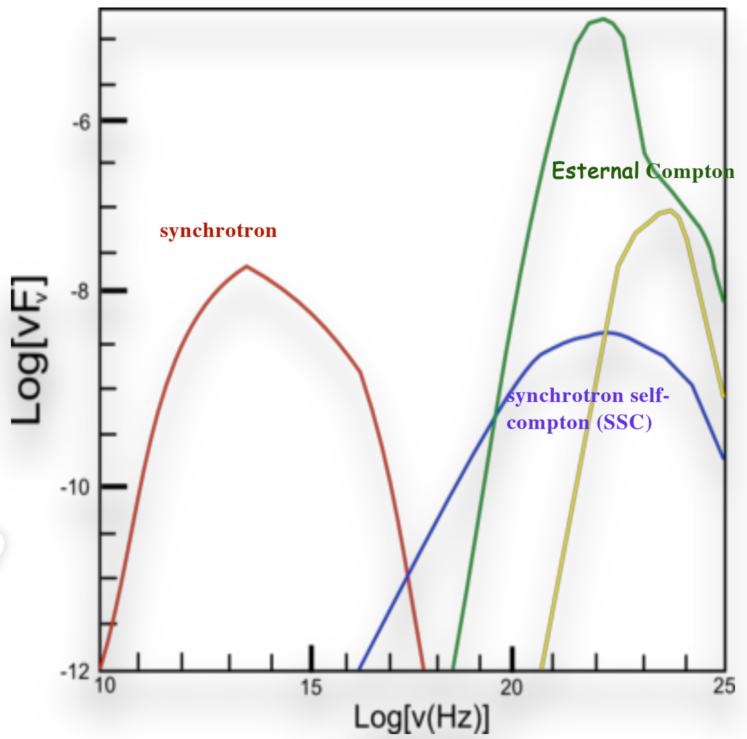

Double-peaked SEDs.III

Abbreviation	Expansion	Probable radio parent	Emission lines
Extreme HBL	TeV blazars (BLL)	Low-luminosity FR-Is	Weak
HBL	High-energy peaked (blue) BLL	FR-I sources	Weak
IBL	Intermediate-energy peaked BLL	FR-I/II break sources	Weak
LBL	Low-energy peaked (red) BLL	Class B FR-IIs	Weak
FSRQ	Flat-spectrum radio quasar	BLRG, FR-II QSR	Strong

Link with neutrino emitters? (the case of TXS 0506+056; Paiano et al. 2018)

BLL: BL Lac object
HBL: high-energy peaked blue BLL
IBL: intermediate-energy peaked BLL
LBL: low-energy peaked BLL

Provides a sort of sequence for the high-energy peak as a function of energy → the second peak (IC) is progressively moving to lower frequencies (thus becoming redder) from HBL to LBL

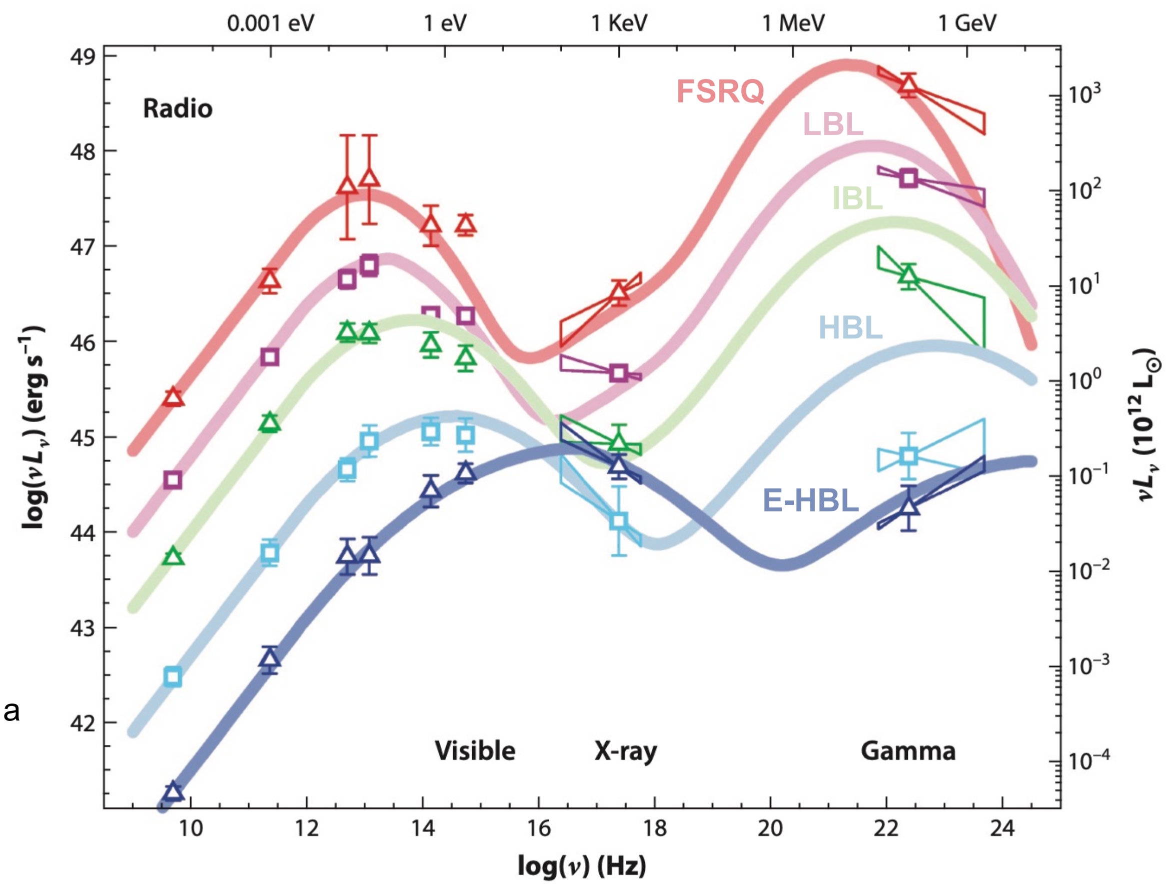

The energy 'dissipated' into radiation is only a minor fraction of the jet power, at least in FSRQs

Blandford et al. (2019, ARAA review)

Double-peaked SEDs.IV

Phenomenological SEDs → implications for possibility of detecting the various classes of blazars at very high energies (e.v. TeV, CTA…)

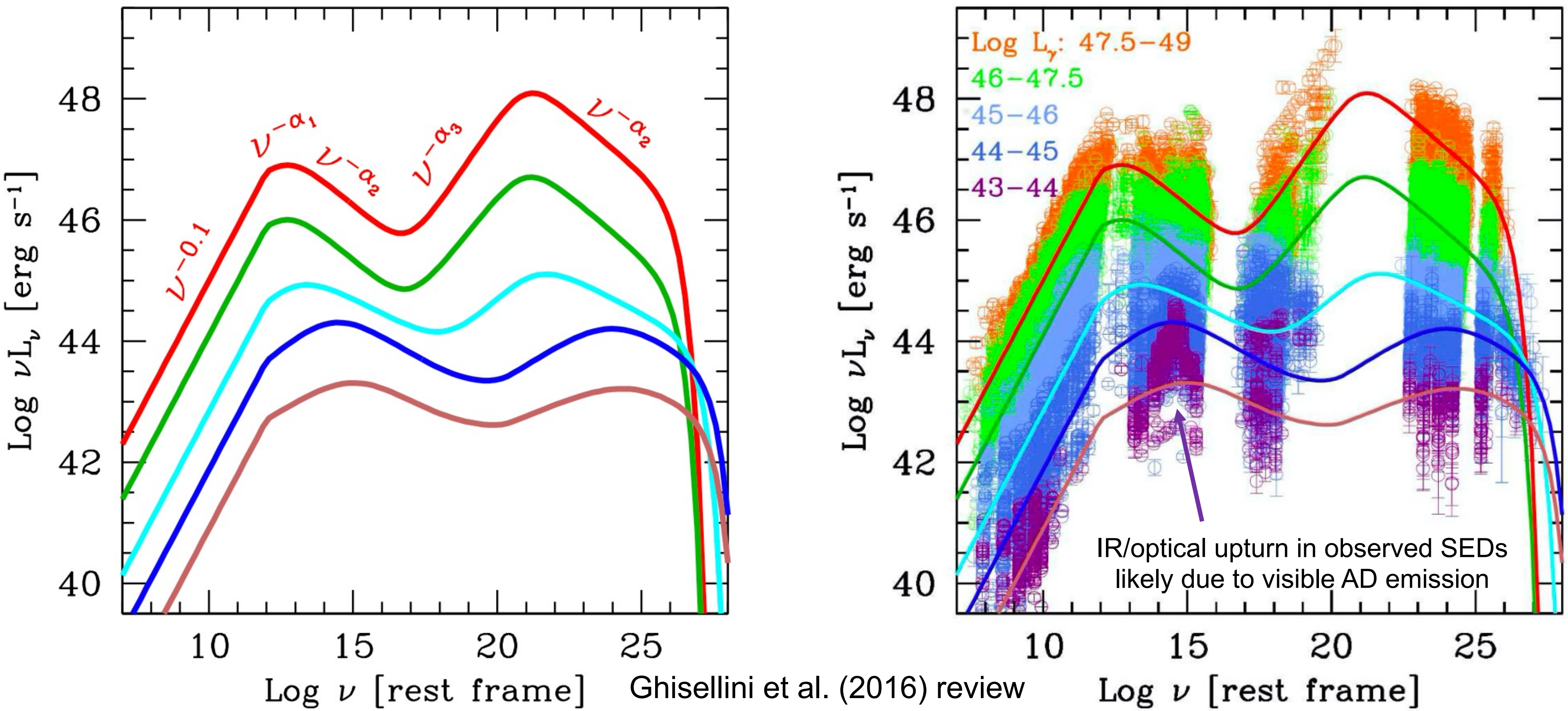

Ghisellini et al. (2016) review

Balance between cooling rate and acceleration rate of the electrons → the most powerful sources (FSRQs) have a large amount of magnetic and radiation energy density, hence strong cooling, not reaching the highest energies of the SEDs (compared to lower-cooling sources as BL Lacs)

Superluminal motions. I

3C273 (z=0.158)

VLBI obs. (Pearson+81,82)
~25 ly over 3-yr

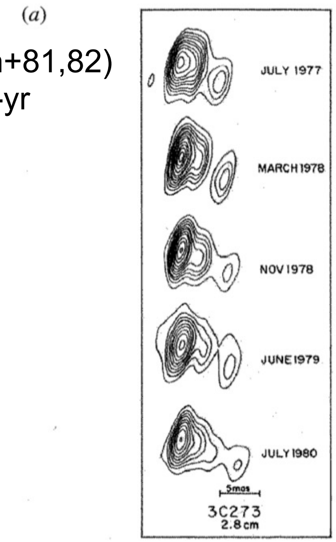

6-yr period motion

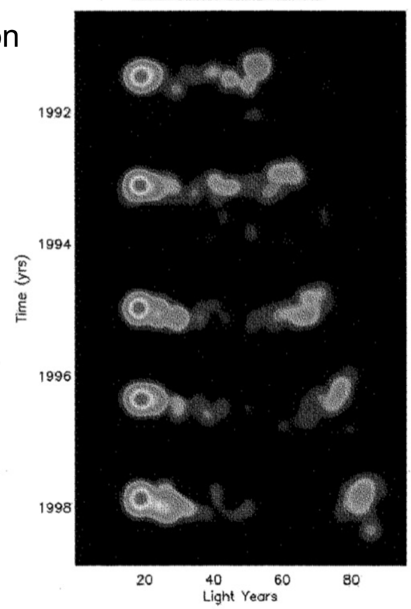

3C120 (z=0.033)

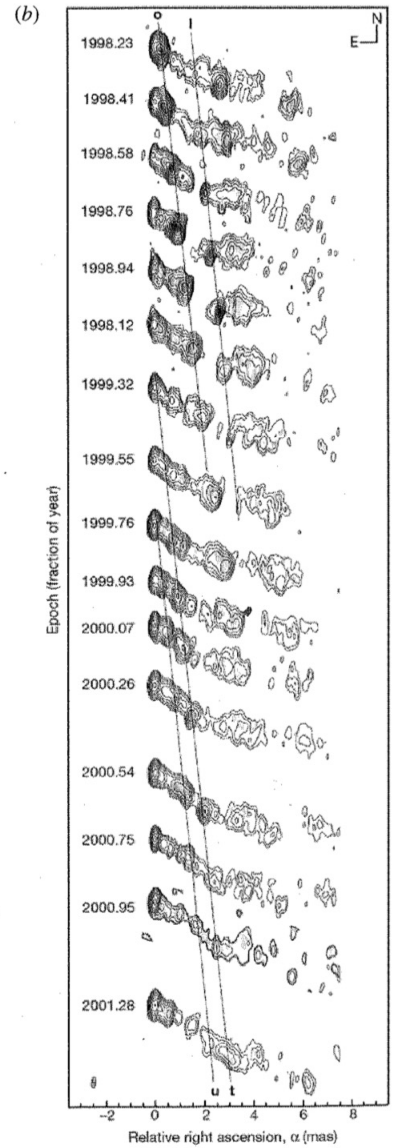

VLBA observations, 16 epochs
v~4.1−5 times the speed of light
(Marscher+02)

Superluminal motions. II

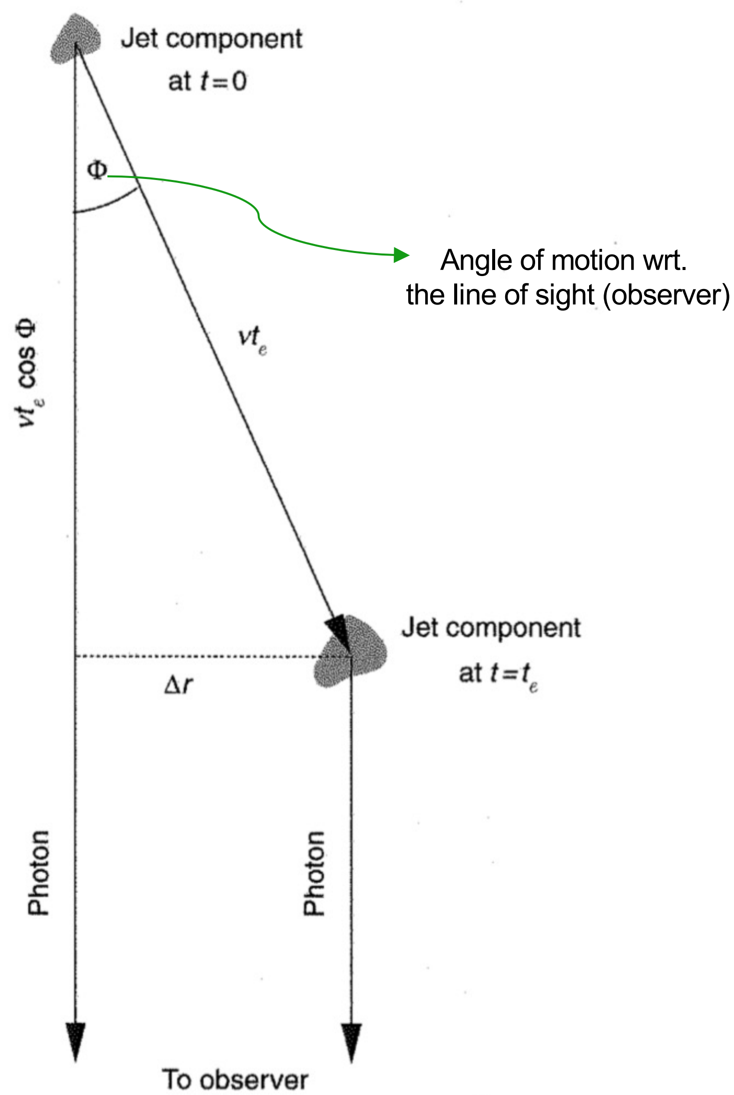

- Very fast motion of the source components at velocity v

$$\Delta r = v\ t_e\ sin\phi$$

observed separation in the tranverse component of **v t$_e$**

- Photons emitted at t=0 and t=t_e will reach us with a time difference of

$$\Delta t = t_e - \frac{v\ t_e\ cos\phi}{c} = t_e(1 - \beta cos\phi)$$

$$v_{app} = \frac{\Delta r}{\Delta t} = \frac{v\ sin\phi}{1 - \beta\ cos\phi}$$

$$(sin\phi)_{max} = \frac{1}{\gamma}$$

$$(v_{app})_{max} = \gamma\ v$$

v_{app} can be >>c

Superluminal motions. III

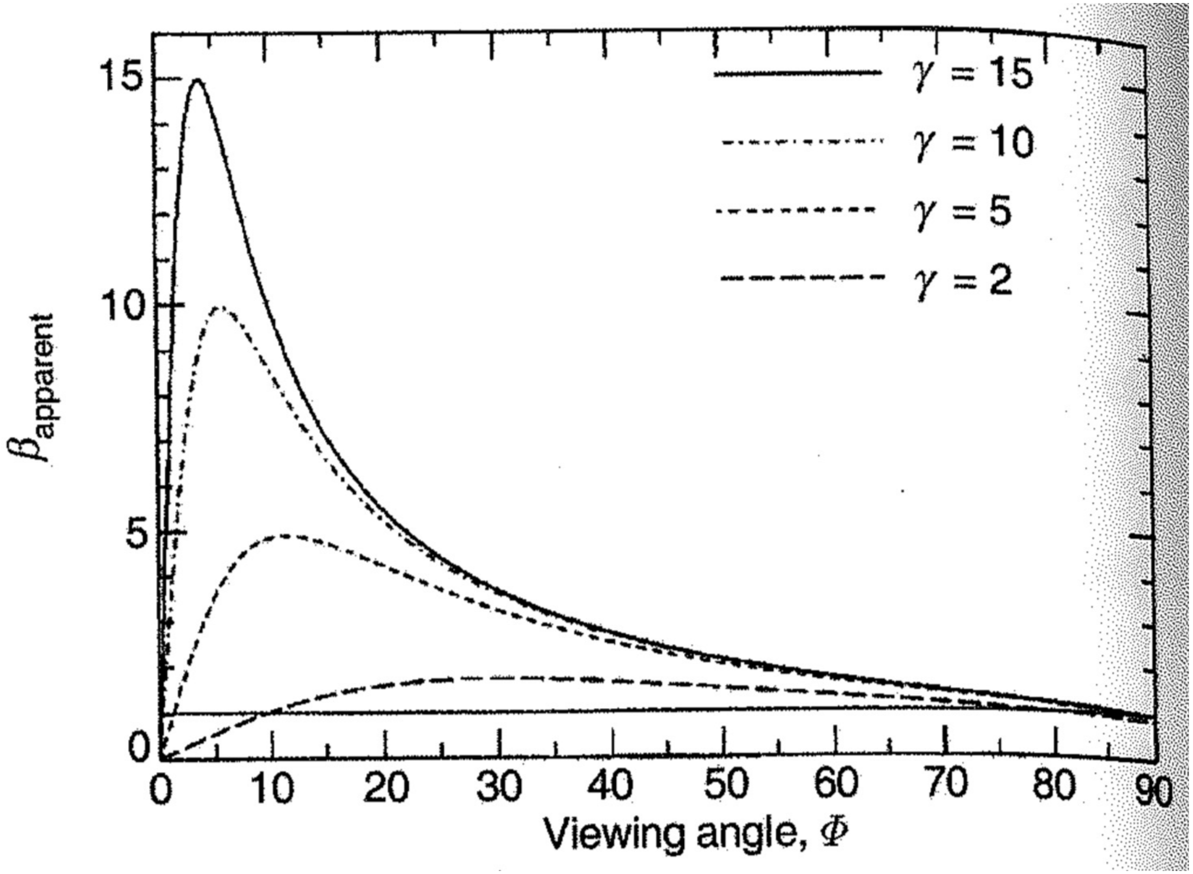

Equipartition. I

$$U_{tot} = U_{el} + U_{pr} + U_M$$

Total energy of a radio source irradiating via synchrotron: energy content in *relativistic particles* and *magnetic field*

$$U_{el} + U_{pr} = (1 + k)\ U_{el}$$

Electrons and B produce the observable radiation. We assume that protons have an energy proportional to U_{el}

$$U_{el} = \int_{E_{min}}^{E_{max}} E\ \underbrace{N(E)\ dE}_{\text{Number density of electrons in the energy E, E+dE}}$$

Energy density of relativistic electrons in the energy range E_{min} to E_{max}

In the case of synchrotron, we have seen that electrons with energy E emit most of the radiation at a frequency

$$\nu \propto\ E^2 B$$

see lessons on emission processes

The electron energy corresponding to the radiation at frequency ν is

$$E \propto B^{-1/2}$$

Equipartition. II

$$-\frac{dE}{dt} \propto B^2 E^2$$

Synchrotron power emitted per electron

$$N(E) \propto E^{-\delta}$$

Electron energy distribution as a powerlaw
δ was reported as *p* in the synchrotron lesson (it is not the Doppler factor described few slides before)

$$L = \int_{\nu_{min}}^{\nu_{max}} L_\nu \, d\nu \propto \int_{E_{min}}^{E_{max}} -(dE/dt) N(E) \, dE$$

Luminosity of a synchrotron source

$$\frac{U_{el}}{L} \propto \frac{\int_{E_{min}}^{E_{max}} E^{1-\delta} dE}{B^2 \int_{E_{min}}^{E_{max}} E^{2-\delta} dE} \propto \frac{E^{2-\delta}\big|_{E_{min}}^{E_{max}}}{B^2 E^{3-\delta}\big|_{E_{min}}^{E_{max}}}$$

Ratio of the electron energy density over the emitted luminosity via synchtrotron emission

E_{max} and E_{min} are proportional to $B^{-1/2}$

$$\frac{U_{el}}{L} \propto \frac{(B^{-1/2})^{2-\delta}}{B^2 (B^{-1/2})^{3-\delta}} = \frac{B^{-1+\delta/2}}{B^2 \; B^{-3/2+\delta/2}} = B^{-3/2}$$

Equipartition. III

$$U_{el} \propto \ B^{-3/2}$$

Electron energy density needed to produce a given synchrotron luminosity

$$U_M \propto \ B^2$$

Magnetic energy density

$$U_{tot} = U_{el} + U_{pr} + U_M = (1+k)U_{el} + U_M \propto \ (1+k)B^{-3/2} + B^2$$

The total energy density U_{tot} has a fairly sharp minimum near **equipartition** (=**same energy content in particles and in magnetic field**)

$$\frac{dU_{tot}}{dB} = \frac{d[(1+k)U_{el} + U_M]}{dB} = 0$$

$$\frac{dU_{el}}{dB}\frac{1}{U_{el}} = -\frac{3}{2}B^{-5/2}B^{3/2} = -\frac{3}{2B} \rightarrow \frac{dU_{el}}{dB} = -\frac{3U_{el}}{2B}$$

$$\frac{dU_M}{dB}\frac{1}{U_M} = \frac{2B}{B^2} = \frac{2}{B} \rightarrow \frac{dU_M}{dB} = \frac{2U_M}{B}$$

Equipartition. IV

$$\frac{dU_{tot}}{dB} = 0 \rightarrow \quad -\frac{3(1+k)U_{el}}{2B} + \frac{2U_M}{B} = 0$$

The total energy is minimized when

$$\frac{\text{Particle energy density}}{\text{Magnetic field energy density}} = \frac{(1+k)U_{el}}{U_M} = \frac{4}{3}$$

The particle energy is close to the magnetic field energy

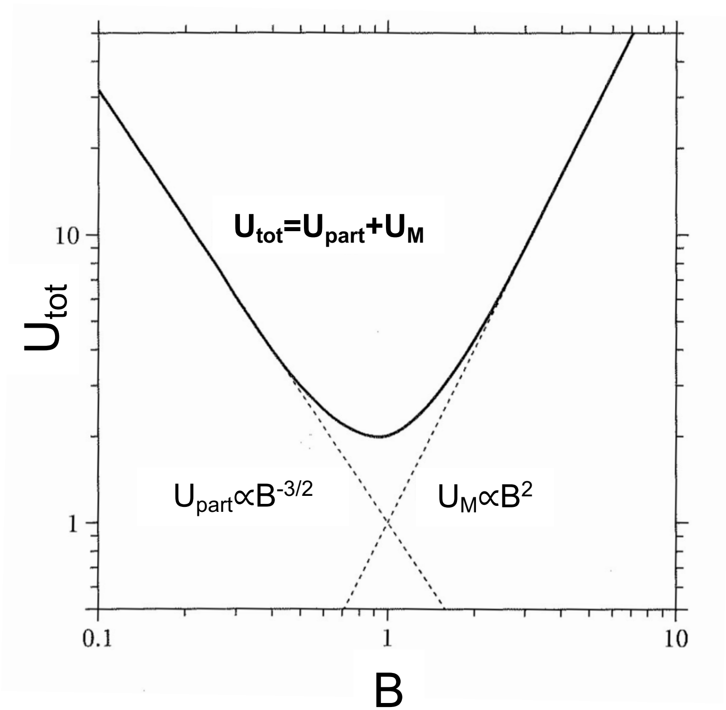

Energy equipartition: condition of minimum energy

Approximately the same energy in particles and magnetic field → Equipartition magnetic field

More on extended structures in RL AGN. I

FRI

For low-luminosity (FRI) radio sources, there is strong support for the *synchrotron process* as the dominant emission mechanism for the X-rays, optical, and radio emission of **jets**

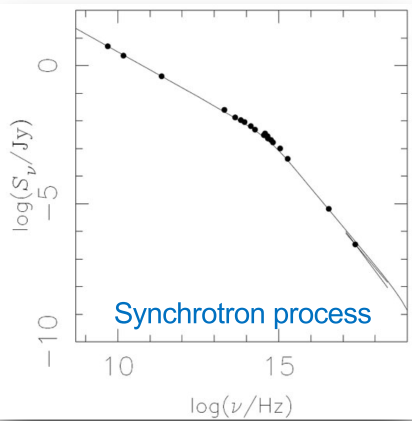

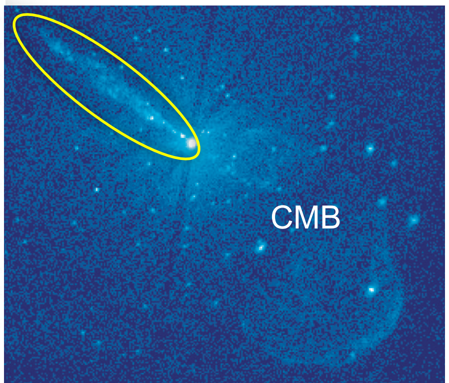

FRII

High-luminosity (FRII) radio sources require multi-zone synchrotron models or synchrotron + IC models (where seed photons are from CMB). Most popular model postulates very fast **jets** with high bulk Lorentz factors

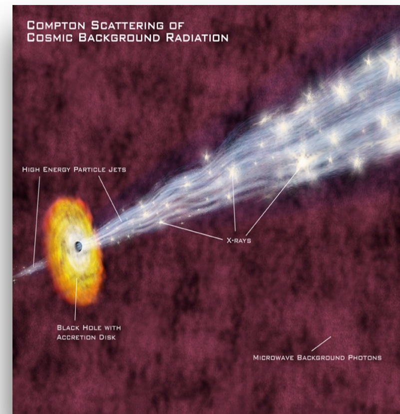

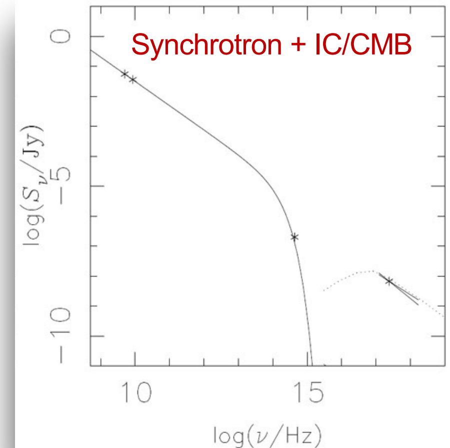

see Harris & Krawczynski (2006, ARAA review)

More on extended structures in RL AGN. II

Lobes

IC scattering by relativistic electrons. Seed photons from either CMB or nuclear photons (the latter case mostly in powerful and compact, R<100 kpc, RGs)

Pictor A (FRII, z=0.035)

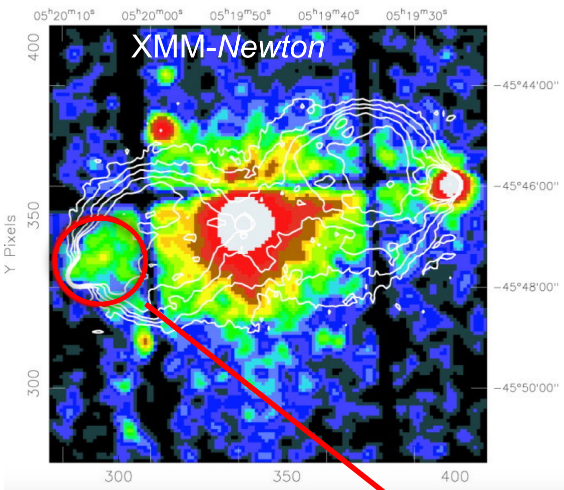

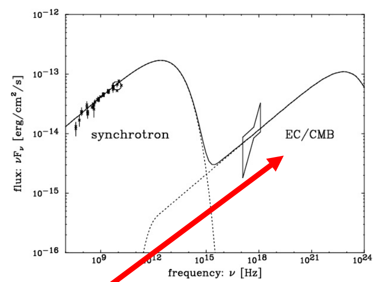

Migliori et al. (2007)

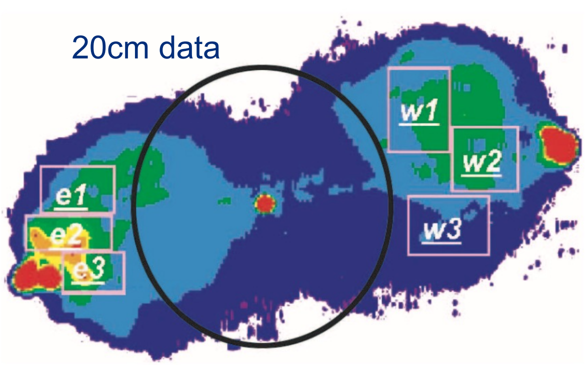

Hot spots

Localized volumes of high emissivity produced by strong shocks. Generally consistent with **SSC** predictions with $B \sim B_{eq}$; cases excess X-ray emission ($B<B_{eq}$? additional component?)